

1 **Aircraft-measured indirect cloud effects from biomass**
2 **burning smoke in the Arctic and subarctic**

3
4 **L. M. Zamora^{1,2}, R. A. Kahn¹, M. J. Cubison³, G. S. Diskin⁴, J. L. Jimenez³, Y.**
5 **Kondo⁵, G. M. McFarquhar⁶, A. Nenes^{7,8,9}, K. L. Thornhill⁴, A. Wisthaler^{10,11},**
6 **A. Zelenyuk¹² and L. D. Ziemba⁴**

7 [1]{NASA Goddard Space Flight Center, Greenbelt, MD, USA}

8 [2]{Oak Ridge Associated Universities, Oak Ridge, TN, USA}

9 [3]{CIRES and Dept. of Chemistry and Biochemistry, University of Colorado, Boulder,
10 CO, USA}

11 [4]{NASA Langley Research Center, Hampton, VA, USA}

12 [5]{National Institute of Polar Research, Tokyo, Japan}

13 [6]{University of Illinois at Urbana-Champaign, Urbana, IL, USA}

14 [7]{Georgia Institute of Technology, Atlanta, GA, USA}

15 [8]{Foundation for Research and Technology - Hellas, Patras, Greece}

16 [9]{National Observatory of Athens, Greece}

17 [10]{Department of Chemistry, University of Oslo, Oslo, Norway}

18 [11]{Institute for Ion Physics and Applied Physics, University of Innsbruck, Austria}

19 [12]{Pacific Northwest National Laboratory, Richland, WA, USA}

20 Correspondence to: L. M. Zamora (laurence@gmail.com)

21
22 **Abstract**

23
24 The incidence of wildfires in the Arctic and subarctic is increasing; in boreal North
25 America, for example, the burned area is expected to increase by 200-300% over the next

1 50-100 years, which previous studies suggest could have a large effect on cloud
2 microphysics, lifetime, albedo, and precipitation. However, the interactions between
3 smoke particles and clouds remain poorly quantified due to confounding meteorological
4 influences and remote sensing limitations. Here, we use data from several aircraft
5 campaigns in the Arctic and subarctic to explore cloud microphysics in liquid-phase
6 clouds influenced by biomass burning. Median cloud droplet radii in smoky clouds were
7 ~40-60% smaller than in background clouds. Based on the relationship between cloud
8 droplet number (N_{liq}) and various biomass burning tracers (BB_t) across the multi-
9 campaign dataset, we calculated the magnitude of subarctic and Arctic smoke aerosol-
10 cloud interactions (ACI, where $ACI = (1/3) * d \ln(N_{liq}) / d \ln(BB_t)$) to be ~0.16 out of a
11 maximum possible value of 0.33 that would be obtained if all aerosols were to nucleate
12 cloud droplets. Interestingly, in a separate subarctic case study with low liquid water
13 content ($\sim 0.02 \text{ g m}^{-3}$) and very high aerosol concentrations ($2000\text{-}3000 \text{ cm}^{-3}$) in the most
14 polluted clouds, the estimated ACI value was only 0.05. In this case, competition for
15 water vapor by the high concentration of cloud condensation nuclei (CCN) strongly
16 limited the formation of droplets and reduced the cloud albedo effect, which highlights
17 the importance of cloud feedbacks across scales. Using our calculated ACI values, we
18 estimate that the smoke-driven cloud albedo effect may decrease local summertime
19 shortwave radiative flux by between $2\text{-}4 \text{ W m}^{-2}$ or more under some low and
20 homogeneous cloud cover conditions in the subarctic, although the changes should be
21 smaller in high surface albedo regions of the Arctic. We lastly explore evidence
22 suggesting that numerous northern latitude background Aitken particles can interact with
23 combustion particles, perhaps impacting their properties as cloud condensation and ice
24 nuclei.

25

26 **1 Introduction**

27 The incidence of wildfires in the Arctic and subarctic is increasing dramatically
28 (Flannigan et al., 2009; Moritz et al., 2012; Stocks et al., 1998), and in some areas, such
29 as boreal North America, it is expected to grow by 200-300% over the next 50-100 years
30 (Balshi et al., 2009). Already, periods of intense wildfires can increase regional aerosol

1 concentrations in the Arctic twofold (Warneke et al., 2010), and the impact of smoke is
 2 increasingly being recognized as a strong contributor to Arctic haze (Hegg et al., 2009,
 3 2010; McConnell et al., 2007; Shaw, 1995; Stohl et al., 2006, 2007). Increases in
 4 biomass burning aerosols could have a large effect on cloud dynamics (Earle et al., 2011;
 5 Jouan et al., 2012; Lance et al., 2011; Lindsey and Fromm, 2008; Rosenfeld et al., 2007;
 6 Tietze et al., 2011); in turn, smoke-derived changes to cloud microphysics may result in
 7 changes to precipitation and regional heating that are strong enough to affect dwindling
 8 regional sea ice (Kay et al., 2008; Kay and Gettelman, 2009; Lubin and Vogelmann,
 9 2006; Vavrus et al., 2010).

10 However, the interactions between smoke particles and Arctic clouds are poorly
 11 quantified, in part due to the confounding effects of meteorology and surface conditions
 12 (e.g., Earle et al. (2011); Jackson et al. (2012); Jouan et al. (2012)), and in part due to
 13 satellite sampling constraints over the Arctic, such as caused by the presence of many
 14 low contrast regions, multi-layer clouds (Intrieri et al., 2002), and reduced sunlight. One
 15 common way in which aerosol-cloud interactions (ACI) are quantified is by assessing
 16 how a cloud property changes relative to some aerosol tracer or, in this case, biomass
 17 burning aerosol tracer (BB_t). Following Eq. (1), ACI estimates for a given location can
 18 be derived from aircraft measurements of cloud droplet number, N_{liq} ; they can also be
 19 derived from ground-based or remote sensing retrievals of changes in cloud properties
 20 such as droplet effective radius (r_e) or cloud optical depth (τ) at constant liquid water path
 21 (LWP) (Feingold et al., 2001; McComiskey et al., 2009):

$$ACI = \frac{1}{3} \frac{d \ln N_{liq}}{d \ln BB_t} = - \left. \frac{\partial \ln r_e}{\partial \ln BB_t} \right|_{LWP} = \left. \frac{\partial \ln \tau}{\partial \ln BB_t} \right|_{LWP} \quad (1)$$

22 The ACI term as defined by Eq. (1) was originally described as the “Indirect Effect” (IE)
 23 (Feingold et al., 2001, 2003). Here, similarly to McComiskey et al. (2009), we use
 24 “ACI” instead of “IE” to differentiate the fact that the metric in Eq. (1) is more directly
 25 associated with aerosol-driven changes to cloud microphysical responses than with
 26 radiative forcing.

27 The maximum value of ACI as derived from Eq. (1) is 0.33. An ACI value of 0.33
 28 corresponds with the 1.0 maximum possible change in $\ln N_{liq}$ relative to $\ln BB_t$, which
 29 would occur if every aerosol were to nucleate a cloud droplet. The first term of Eq. (1) is

1 divided by 3 in order to correspond with the last two terms, which are derived at constant
2 LWP from the following theoretical relationships: $r_e \propto \text{LWP}/\tau$ (Stephens, 1978) and $\tau \propto$
3 $N_{\text{liq}}^{1/3}$ (Twomey, 1977). Note that although each term in Eq. (1) should equal each other
4 term, in practice measurement-derived biases can cause apparent differences between the
5 terms. This issue will be discussed further in later sections.

6 One study convincingly demonstrated that smoke reduces cloud droplet effective radius
7 and enhances cloud albedo in Arctic liquid clouds (Tietze et al., 2011). In that study,
8 modeled BB_t concentrations were combined with remote sensing of cloud properties,
9 enabling the authors to reduce meteorological bias by basing their conclusions on tens of
10 thousands of clouds sampled over a variety of meteorological conditions throughout the
11 Arctic. Smoke ACI values derived from relative changes in cloud r_e were estimated at
12 between 0.04-0.11 out of a maximum 0.33. (Note however that in that study, clouds were
13 binned by temperature and pressure, rather than by LWP as in Eq. (1) above.)

14 However, despite being able to conclusively demonstrate a smoke cloud albedo effect,
15 Tietze et al. (2011) noted that they might have underestimated the magnitude of satellite-
16 derived ACI values because of difficulties constraining aerosol concentrations and
17 locations. They cite a study by Costantino and Breón (2010), where it was demonstrated
18 that not co-locating aerosol-cloud layers in the vertical column dramatically lowered ACI
19 estimates from 0.24 to 0.04 over marine stratocumulus clouds influenced by African
20 biomass burning. This bias seems to be apparent in many ACI estimates globally; from a
21 literature search, McComiskey and Feingold (2012) revealed that remote sensing-derived
22 ACI values worldwide are lower than those derived from in-situ, modeling and/or
23 ground-based studies. They also showed that in addition to errors in co-location of
24 clouds and aerosols, the comparatively low spatial resolution of remote sensing
25 observations can further enhance the low bias in ACI estimates.

26 In the Arctic, these biases can be substantial. In a study in Northern Finland, ACI
27 estimates derived over the same general time period and location from both ground-based
28 and remote sensing methods were ~ 0.25 and 0.09 ± 0.04 , respectively (Lihavainen et al.,
29 2010); a more than two-fold difference. For reference, the range of Arctic remote
30 sensing-derived ACI estimates for all aerosol sources is -0.01 to 0.09 (Lihavainen et al.,

1 2010; Tietze et al., 2011); in situ, ground-based, and model estimates range between
2 0.05-0.3 (Garrett et al., 2004; Lihavainen et al., 2010; Zhao et al., 2012). The degree of
3 bias at other global sites has led McComiskey et al. (2012) to assert that the albedo effect
4 can only be assessed accurately from aircraft or ground-based in situ data.

5 To better understand the impacts that expected increases in smoke will have on the
6 Arctic, it is important to better constrain remote-sensing and model estimates of smoke-
7 specific ACI in the Arctic using in situ aircraft data. The biggest challenge in obtaining
8 representative aircraft-based ACI values is the fact that they are more prone to
9 uncertainties caused by the influences of poorly constrained meteorological factors (Shao
10 and Liu, 2006) than other methods due to logistical limitations in sample size. We
11 confront this issue in two ways. First, we focus on a case study day from the Arctic
12 Research of the Composition of the Troposphere from Aircraft and Satellites (ARCTAS)
13 campaign (Fuelberg et al., 2010; Jacob et al., 2010) in which several clouds were sampled
14 under very similar conditions. We derive ACI estimates for all clouds that were either
15 verifiably clean or are clearly influenced by biomass burning aerosols, and contrast the
16 observed cloud properties. Second, to increase sample size, we consolidated data from
17 four separate aircraft campaigns in the Arctic. In addition to ARCTAS, these datasets
18 include: the First ISCCP (International Satellite Cloud Climatology Project) Regional
19 Experiment Arctic Clouds Experiment (FIRE.ACE), which included portions flown by
20 the University of Washington Convair-580 (UW FIRE.ACE) and the Canadian National
21 Research Council Convair-580 (NRC FIRE.ACE) (Curry et al., 2000), and the Indirect
22 and Semi-Direct Aerosol Campaign (ISDAC) (McFarquhar et al., 2011). We then
23 compare these findings with those from the ARCTAS case study.

24

25 **2 Methods**

26 **2.1 Dataset description**

27 The dates and flight locations of data used in this study are shown in Fig. 1, and the data
28 used are listed in Tables 1-4. The ARCTAS, FIRE.ACE, and ISDAC datasets have each
29 been extensively described previously (e.g., Curry et al., 2000; Fuelberg et al., 2010;
30 Jacob et al., 2010; Korolev et al., 2003; McFarquhar et al., 2011; Rangno and Hobbs,

1 2001; Soja et al., 2008). However, to our knowledge, they have never been compared
2 directly to each other. Here we note only briefly a few relevant points about the datasets
3 and how they are inter-compared.

4 First, during the ISDAC and FIRE.ACE flights, multiple passes inside clouds were often
5 obtained, and aerosols were intentionally sampled above- and below-cloud. In contrast,
6 during ARCTAS there was very limited resampling of a given region and generally only
7 one pass through a cloud was obtained. This difference in sampling impacts our results
8 only in that there are not as many vertical profiles through the ARCTAS clouds as in the
9 other datasets. Second, the UW FIRE.ACE dataset contains some gaps in positional data
10 (latitude, longitude, and altitude), which range most frequently between 1-10 seconds,
11 with rare instances of gaps >1 minute. If the data were out-of-cloud and if the gap in
12 positional data is <1 minute, we linearly interpolate the latitude, longitude, and/or
13 altitude. Otherwise, occasional gaps > 1 minute and data without positional information
14 were excluded. Thirdly and most importantly, we have made our best effort to use data
15 that are as comparable as possible between campaigns. However, when high quality
16 measurements are not available from the same instrument in all campaigns, we use the
17 most similar measurement available and we discuss the uncertainties this raises in the
18 text.

19 **2.2 Cloud presence and phase**

20 **2.2.1 ARCTAS**

21 In ARCTAS, cloud liquid water content (LWC) was determined from droplet size spectra
22 gathered with the CAPS-CAS instrument (Baumgardner et al., 2001) based on integrated
23 volume droplet size distributions between 0.75-50 μm . Throughout this size range,
24 precision was estimated to be 20% within each size bin based on pre-calibrations with
25 sized glass and polystyrene latex spheres. We expect accuracy to also be ~20%, since
26 pre-campaign calibrations were performed with spheres of known size, and since post-
27 campaign tests with latex spheres were consistent with the expected sizes. Unfortunately,
28 we could not validate in situ accuracy because simultaneously collected hot-wire probe
29 LWC data were unobtainable due to high noise in out-of-cloud samples. For this reason,
30 in-cloud hot-wire LWC data are not reported here other than to note that they showed

1 qualitatively consistent trends with the CAPS-CAS LWC data. Liquid phase cloud
2 presence was defined by LWC values $\geq 0.01 \text{ g m}^{-3}$ (Matsui et al., 2011b), a value that
3 corresponds well with cloud presence verified from the on-flight video. Because neither
4 ice water content (IWC) nor cloud particle images were directly measured during
5 ARCTAS, we are unable to accurately verify cloud phase at temperatures $< 0 \text{ }^\circ\text{C}$ in the
6 ARCTAS dataset. Therefore, we limited our focus within the ARCTAS dataset to clouds
7 present at temperatures $> -0.5 \text{ }^\circ\text{C}$ (i.e., those clouds highly likely to be in the liquid
8 phase). We also excluded clouds that video indicated were affected by drizzle or ice
9 precipitation from cloud layers above.

10 **2.2.2 FIRE.ACE and ISDAC**

11 During the UW and NRC FIRE.ACE campaigns, LWC was determined from droplet size
12 spectra gathered from Forward Scattering Spectrometer Probe (FSSP-100) measurements
13 for particles with diameters between $0.5\text{-}47 \text{ }\mu\text{m}$ and $5\text{-}47 \text{ }\mu\text{m}$, respectively. These
14 measurements are functionally very similar to the CAPS CAS measurements from
15 ARCTAS. During the sampling periods where air mass classification matched the criteria
16 described in section 2.4, the FSSP data had a close relationship to hot-wire probe
17 measurements of LWC for both campaigns (Table 5). For the NRC FIRE.ACE
18 campaign, two FSSP probes were available (serial numbers 96 and 124, denoted hereafter
19 as FSSP-96 and FSSP-124). The FSSP-96 is normally recommended for use by the data
20 originators because the FSSP-124 had an intermittent hardware problem during the NRC
21 FIRE.ACE campaign, and because it may have undersized particles $>30 \text{ }\mu\text{m}$ diameter.
22 In this analysis, the hardware problem did not occur during our time periods of interest,
23 and the FSSP-124 droplet distribution for droplets with diameters within $30\text{-}47 \text{ }\mu\text{m}$
24 closely matched those of the FSSP-96. However, the FSSP-124 had higher droplet
25 numbers in particles with diameters $< 30 \text{ }\mu\text{m}$ compared to the FSSP-96 during the
26 relevant sampling periods used in this study. We believe this discrepancy to be due to a
27 deficiency in the FSSP-96 data during this time period, because the FSSP-96
28 underestimated King and Nevzorov probe LWCs by $\sim 23\%$ and 26% , respectively,
29 whereas the FSSP-124 data estimated King and Nevzorov probe data to within 8% , on

1 average (Table 5). Therefore, the FSSP size distribution data reported here for the NRC
2 FIRE.ACE campaign are based on FSSP-124 data between 5-47 μ m.

3 During ISDAC, LWC was determined from cloud droplet probe (CDP) data. These data
4 agreed within 15% of the bulk probe values. Following Earle et al. (2011), FSSP data
5 were used on days when high-quality CDP data were unavailable; the FSSP data are
6 estimated to agree with CDP data to within 20%. Note that similarly to ice particles (e.g.,
7 Korolev et al. (2011)), very large droplets may shatter on any of the cloud droplet probe
8 tips. This may introduce some potential artifacts when droplet sizes are very large (e.g.,
9 for some of the reference measurements available in FIRE.ACE and ISDAC).

10 For comparability with ARCTAS clouds, the presence of liquid clouds in the FIRE.ACE
11 and ISDAC datasets was determined by simultaneous measurements of $LWC > 0.01 \text{ g m}^{-3}$
12 ³. Also, for inter-campaign comparisons we focused on clouds sampled for ≥ 20 s in
13 order both to increase representativeness of the average measured properties of the clouds
14 and to enhance meteorological similarity of clouds. Sometimes entrainment from outside
15 air caused pockets of low- to no-LWC (i.e., $LWC < 0.001 \text{ g m}^{-3}$) within a cloud body;
16 these pockets of air were not included when determining the average cloud droplet
17 effective radius.

18 There is no consistent definition for cloud phase in the literature. In remote sensing
19 studies for example, cloud phase is usually determined by cloud radiative properties –
20 thus, clouds with some mixed particles can be included in “liquid” or “ice” phase
21 classifications if they are mostly liquid or mostly ice (e.g., Baum et al. (2012), Platnick et
22 al. (2003)). Due to instrumentation limitations, aircraft studies sometimes also define a
23 cloud with small fractions of ice particles as being a “liquid” cloud (e.g., Korolev et al.
24 (2003)). Alternatively, distinct portions of a cloud may be classified as different phases if
25 a primarily liquid portion of a cloud is far away ($\sim 1\text{-}2$ km) from a mixed portion of a
26 cloud mass (McFarquhar et al., 2007; Zuidema et al., 2005).

27 Here, we define liquid cloud phase by the lack of any ice particles in the CPI data
28 throughout the entire cloud transect, based on a roundness criterion (Lawson et al., 2001).
29 When possible (i.e., in the NRC FIRE.ACE and ISDAC datasets), we verified that there
30 was no detectable ice water along the cloud transects. This relatively stringent definition

1 of liquid phase clouds is used to describe as best as possible the liquid phase end-member
2 cloud characteristics. Because aircraft cloud transects can only sample a portion of a
3 cloud, we must assume that the portion of the cloud sampled is representative of the rest
4 of the cloud. This may introduce uncertainties, particularly in persistent large-scale
5 stratus clouds. Nonetheless, as discussed in Sect. 3.1, we believe that errors from this
6 assumption are not likely to have a large impact on our results.

7 **2.3 Cloud microphysical properties**

8 We used aircraft vertical profiles to assess cloud droplet effective radius (r_e), cloud liquid
9 water path (LWP) and cloud optical depth (τ), and to gather information on aerosol
10 properties above and below cloud. The r_e was derived by Eq. (2), following Hansen and
11 Travis (1974):

$$r_e = \frac{\int r^3 n(r) dr}{\int r^2 n(r) dr} \quad (2)$$

12 where r is the radius, and $n(r)$ is the cloud particle size distribution. LWP is defined as
13 the vertical integral of LWC from the base to the top of the cloud. LWP values were only
14 determined when vertical profiles through the cloud were available, thus providing the
15 cloud base and top heights. We define τ following Peng et al. (2002) as:

$$\tau = \frac{3}{2} \frac{LWC H_c}{r_e \rho_w} \quad (3)$$

16 where H_c is cloud thickness (again only available in vertical cloud transects) and ρ_w is the
17 density of water. In addition to vertical transects, we also used horizontal transects
18 within clouds to obtain information on horizontal variability of within-cloud properties
19 and to obtain increased sample numbers for r_e .

20 In some instances in the multiple-campaign analysis, the same cloud or very
21 similar clouds were sampled more than once, often intentionally, either through an entire
22 vertical cloud transect or through a portion of a cloud. In order to reduce the potential for
23 pseudo-replication in the analysis, transects that were deemed to be from the same cloud
24 or from very similar clouds were averaged to provide one aggregated profile or r_e and N_{liq}
25 value for those instances. Clouds were determined as being related in part by a

1 combination of time and location sampled. Here, the range of distance and time between
2 clouds deemed as related or the same ranged from 0.4 -76 km and several seconds to 2.5
3 hours apart, depending on the conditions and cloud type (the 2.5-hour time frame
4 included 8 separate transects through a stratus cloud). In addition, in all clouds we
5 assessed cloud pressure, location, temperature, and on-flight video (when available). In
6 biomass burning cases we also assessed nearby aerosol conditions (as determined in
7 ISDAC by SPLAT II particle composition and in ARCTAS by CH₃CN, black carbon
8 (BC), submicron SO₄²⁻ and submicron organic aerosol, or OA, concentrations). Within the
9 multi-campaign analysis, 2 of the 8 biomass burning clouds contained aggregated
10 transects, as did 4 of the 16 background clouds. One background cloud in the case study
11 included aggregated transects. To assess the impact of cloud transect aggregation on our
12 analysis, we calculated differences in ACI values using the maximum and minimum
13 values of N_d within the aggregated samples. Calculated differences in ACI values were
14 1%, indicating that uncertainties caused by aggregation had only minor impacts on our
15 results.

16 LWC among aggregated clouds was generally similar (within 30% of each other).
17 However, in some cases it was more variable; in one biomass burning aggregation, the set
18 of 8 related cloud transects had LWCs ranging from 0.12-0.54 g m⁻³. The relationship of
19 LWC with r_e suggests that entrainment could have influenced LWC variability within this
20 particular cloud. Although we cannot constrain the influence of entrainment to a high
21 degree of certainty within an individual cloud aggregate, as discussed in section 3.1, the
22 ACI values derived across all clouds did not deviate from adiabatic values calculated
23 from cloud parcel theory.

24 **2.4 Air mass classification**

25 For this work, distinguishing smoke-influenced from background cloud conditions is
26 critical. During ARCTAS, background conditions were selected by a combination of in-
27 cloud gas concentrations (average CO < 123 ppbv and average acetonitrile (CH₃CN) <
28 0.14 ppbv) and near-cloud SO₄²⁻ and BC concentrations (< 0.3 μg m⁻³ and < 0.12 μg C m⁻³,
29 respectively). In ideal cases, “near-cloud” air masses were defined as half the width of
30 the cloud if it was a vertical profile, and within 10 s before and after the cloud if it was a

1 horizontal transect. However, sometimes the presence of a neighboring cloud or the
2 vertical changes in the aircraft track forced us to use slightly smaller samples.

3 The 123 ppbv CO cutoff value represents the upper quartile range of time periods with
4 concurrently low CO, CH₃CN, and BC (all separate indicators of combustion), and the
5 CH₃CN cutoff is the median for these values. For comparison, Latham et al. (2013) and
6 Moore et al. (2011) defined background air masses as having CO and CH₃CN values at
7 <170 ppbv and 0.1 ppbv, respectively, and Lance et al. (2011) used a criterion of ~160
8 ppbv CO. Such high background CO values are observed periodically over springtime
9 Alaska due to higher emissions from Asia during spring and reduced photochemical loss
10 during winter months (Brock et al., 2011). In 2008 specifically (during a similar time
11 period as ARCTAS-A), background CO was elevated further due to unusually early and
12 frequent Asian wildfires that year (Moore et al., 2011). However, background Arctic CO
13 levels can frequently be lower than these values. For example, during a separate summer
14 campaign in 2011 over eastern Canada, Sakamoto et al. (2015) observed and used a lower
15 background CO threshold of 120 ppbv. Our chosen CO threshold of 123 ppbv, was
16 chosen in part because it enabled the use of a consistent value to characterize background
17 conditions across the wide temporal and spatial region covered during ARCTAS.

18 ARCTAS “biomass burning” influenced air masses were classified following the
19 procedure of Latham et al. (2013), where BB-influenced air masses have concentrations
20 of >175 ppbv and 0.2 ppbv CO and CH₃CN, respectively. A manual scan indicated that
21 aerosol pollutant tracers BC and submicron SO₄²⁻ were always elevated with respect to
22 background concentrations under these conditions in this dataset. For comparison, Lance
23 et al. (2011) used a concentration of >200 ppbv CO for “polluted” (mostly biomass
24 burning) cases.

25 During the two FIRE.ACE campaigns, the combination of relevant high-quality and/or
26 high-resolution aircraft chemical data for completely characterizing air mass sources
27 were not collected, and remote sensing products useful for air mass classification were
28 also unavailable. As a result, biomass burning-derived haze events were
29 indistinguishable from anthropogenic pollution events in the FIRE.ACE datasets.

1 Therefore, we only use FIRE.ACE clouds sampled under non-polluted background
2 conditions for inter-comparison with the other datasets.

3 Because within-cloud gas concentrations were not available, we used average near-cloud
4 (as defined above) aerosol concentrations to define “background” conditions in the
5 FIRE.ACE data. To reduce the risk of any potential humidification effects, we excluded
6 near-cloud air masses that had any observations of cloud particles in the CPI or that had
7 LWC values $\geq 0.001 \text{ g m}^{-3}$.

8 To classify background air masses, we used Passive Cavity Aerosol Spectrometer Probe
9 (PCASP) aerosol concentrations (CN_{PCASP}) directly adjacent to the cloud. The PCASP
10 measures dehumidified particles with diameters between 0.12-3 μm . Previous authors
11 have noted the presence of large numbers of small nucleation- to Aitken-mode particles
12 (between $\sim 15\text{-}85 \text{ nm}$) in the spring- and summer-time Arctic that appear to have natural
13 sources (Garrett et al., 2004; Howell et al., 2014; Leitch et al., 2013; Leck and Bigg,
14 1999; O’Dowd et al., 2010; Ström et al., 2009; Tunved et al., 2013; Zhao and Garrett,
15 2015). However, the relatively large minimum size cutoff of the PCASP ($\sim 120 \text{ nm}$)
16 excludes these particles, while including low altitude particles from pollution and
17 biomass burning sources, which tend to be in the accumulation mode (Earle et al., 2011;
18 Latham et al., 2013; Warneke et al., 2010). Thus, CN_{PCASP} tends to be a fairly good
19 indicator of non-background conditions.

20 To be classified as background, air masses had to have CN_{PCASP} concentrations of ≤ 127
21 particles cm^{-3} (Shantz et al., 2012). This CN_{PCASP} cutoff is a more stringent criterion for
22 determining clean conditions than those adopted by Jackson et al. (2012), Earle et al.
23 (2011) and Peng et al. (2002), where respective values of < 200 , 250 and 300 particles
24 cm^{-3} were used, but the criterion applied here appears to exclude biomass burning and
25 pollution aerosols fairly effectively (Table 6). However, the upper 95% CH_3CN
26 concentrations are higher than typical background conditions, indicating that our chosen
27 cutoff value is generally, but not completely, effective at removing air masses influenced
28 by smoke. Therefore, the FIRE.ACE samples have a more uncertain background
29 classification than the ARCTAS and ISDAC datasets, where actual chemical tracers
30 verify the presence of pollution and biomass burning aerosols. For ISDAC samples,

1 “background” conditions were determined by out-of-cloud CN_{PCASP} concentrations, in
2 order to be consistent with the FIRE.ACE campaigns. However, the TSI aerosol
3 concentrations (CN_{TSI}) and backscatter values were not used to assign a background
4 classification (see Sect. 3.2 for further details).

5 A “biomass burning” classification was assigned in ISDAC data when a cloud had
6 contact with discernable amounts of biomass burning aerosols, as determined by single
7 particle mass spectrometer, SPLAT II (Zelenyuk et al. 2009; Zelenyuk et al. 2015), based
8 on the mass spectral analysis of individual aerosol particles (Fig. 2). This method has
9 been similarly employed to determine biomass burning influence in the ISDAC dataset
10 previously (Earle et al., 2011; McFarquhar et al., 2011; Shantz et al., 2014).

11 **2.5 Assessment of indirect effects from biomass burning**

12 As mentioned before, the impact of smoke aerosols on cloud droplet activation was
13 assessed by looking at aerosol-cloud interactions (ACI) of biomass burning aerosols on
14 cloud droplet number. The ACI values were derived from changes in cloud droplet
15 number relative to measured biomass burning tracers, BB_t , following Eq. (1) and using a
16 non-parametric Kendall robust line-fit method. The Kendall robust line-fit model (also
17 commonly known as the Theil-Sen method) (Sen, 1968; Theil, 1950) derives a linear
18 model of a dataset from the median of the slopes between each two points in the dataset.
19 While this method is not as commonly used as linear regressions, it performs similarly
20 when data are normally distributed. In cases when the data are not normally distributed,
21 this method is more appropriate than a linear regression because it reduces the impact of
22 outliers.

23 As previously mentioned, ARCTAS was the only campaign where biomass burning
24 gaseous tracers were directly quantifiable in-cloud (here we use $BB_t = CH_3CN$ (de Gouw
25 et al., 2003) and $BB_t = CO$ (Tietze et al., 2011)), measured in ppbv. Both CO (Bian et al.,
26 2013) and CH_3CN have appreciable background concentrations in the Arctic (as can be
27 seen in Fig. 3a). Therefore, approximate background CO and CH_3CN concentrations of
28 99.2 and 0.088 ppbv, respectively, were subtracted prior to deriving ACI values from Eq.
29 (1) in the case study. These background values were derived from the mean of the
30 Kendall robust line-fit method analyses of ARCTAS CCN and CN_{PCASP} equivalent

1 concentrations vs. CO (or CH₃CN) concentrations. In the multi-campaign analysis,
2 background values of 0.018 ppbv CH₃CN were subtracted, due to lower background
3 concentrations in the cleanest samples. Although for simplicity we define a single
4 background Arctic CH₃CN level here, background CH₃CN can range from ~0.050 ppbv
5 in the Arctic marine boundary layer to ~0.14 ppbv at altitudes of ~8 km (Kupiszewski et
6 al., 2013; Warneke et al., 2009; A. Wisthaler, personal communication, 2015). A
7 maximum error of 0.038 ppbv in background CH₃CN would equal at most 18% of the
8 CH₃CN signal in biomass burning samples. For that reason, and because CH₃CN was
9 only one of six tracers used to derive ACI values, the range of possible background
10 CH₃CN concentrations is expected to have only minor impacts on the analysis. Arctic
11 background CO is more consistent than CH₃CN, and in that case, the differences in
12 background CO as computed from CN_{PCASP} vs. CCN line-fit analyses (93.0 and 105.4
13 ppbv, respectively) led to only a 2.6% change in the derived ACI values.

14 Because the in-cloud CO and CH₃CN values were not available in the ISDAC or
15 FIRE.ACE campaigns, we also compared aerosol tracers of smoke/polluted particles
16 adjacent to the cloud as a BB_t quantity. The aerosol tracers used were CN_{PCASP}
17 concentrations, backscatter at 550 nm, BC concentrations, and when available, CCN (not
18 available in the UW FIRE.ACE campaign). For comparison to the PCASP, aerosol
19 concentrations with diameters > 4 nm were measured with a TSI 3775 in ISDAC.
20 Aerosols with diameters > 3 and 10 nm were measured during ARCTAS from TSI
21 models 3025 and 3010, respectively. Because CN_{PCASP} values were not measured during
22 ARCTAS, we combined APS and UHSAS sized aerosol data collected during that
23 campaign into a similar size distribution as the CN_{PCASP} measurements (0.124-3.278 μm).
24 UHSAS and APS measurements are not actively dried like PCASP samples are (Earle et
25 al., 2011; Strapp et al., 1992), but sample humidity decreases significantly upon heating
26 in the cabin and measurements are taken at dry relative humidity; in addition, particles
27 are exposed to dried sheath air prior to detection.

28 There are some limitations of the ACI approach. First, a systematic bias can be
29 introduced when aerosol and cloud properties are averaged or co-located in low spatial or
30 temporal resolution datasets (McComiskey and Feingold, 2012). This particular
31 systematic bias is generally not a large concern for in-cloud aircraft studies such as this

1 one where gas and/or aerosol measurements and N_{liq} measurements are either collected
2 simultaneously or in very close proximity. Secondly, the magnitudes of derived ACI can
3 vary depending on the BB_t tracers used, and any one tracer may be biased by random
4 error and a variety of other reasons that may cause the tracer to imperfectly approximate
5 actual cloud droplet nuclei. To reduce the biases inherent to any one tracer, we use a
6 combination of up to six BB_t tracers to derive ACI, as available.

7 A third potential problem is the risk that a snapshot of a cloud in time is not
8 representative of the net cloud properties over its lifetime (Duong et al., 2011).
9 Currently, only models can fully characterize cloud lifetime properties, but interpreting
10 the model output can be challenging for other reasons. Within aircraft in situ data, this
11 source of sampling error is best minimized in aircraft in situ data by resampling
12 throughout the cloud's life cycle. Resampling was sometimes, but not always, carried out
13 for individual cloud cases presented here, and was not specifically carried out throughout
14 the lifetime of the cloud. However, based on the results presented in Duong et al. (2011),
15 the magnitude of this type of error is unlikely to have a large impact on our results,
16 although we cannot with full confidence assess how cloud life stage might have impacted
17 the way aerosols were interacting with the clouds.

18 The fourth limitation with the ACI method is that N_{liq} has a sublinear relationship with
19 CCN (e.g., Morales et al. [2011]; Morales and Nenes [2010]), with particularly noticeable
20 deviations from linear behavior expected when a cloud contains high CCN concentrations
21 (e.g., Moore et al. [2013]). This behavior is driven by increased competition for water
22 vapor, which in turn decreases cloud supersaturation and reduces the tendency to form
23 additional drops. Because ACI values are typically derived from linear-type regressions,
24 apparent ACI values can be reduced if clouds with high CCN are included in the analysis.
25 We discuss the potential for this type of interaction where applicable in the text. Finally,
26 the most difficult problem to address is the potential bias introduced if one does not
27 account for meteorological conditions (Shao and Liu, 2006). We discuss the relationship
28 of derived ACI with meteorology in sections 2.6 and 3.

29 **2.6 Overview of surface and meteorological conditions**

30 Ambient conditions such as cloud type and presence of drizzle from an overlying cloud

1 deck were determined from available video, photos, flight notes and AVHRR images.
2 Although in situ chemical and physical measurements were primarily used to determine
3 end-member situations (i.e., where only smoke or only background air were the dominant
4 sources of aerosols interacting with clouds), in some cases we discuss out-of-cloud
5 aerosols with potentially more mixed sources. In these cases we supplemented chemical
6 and physical data with 5-day HYSPLIT back trajectories (Draxler, R.R. and Rolph, G.D.
7 HYSPLIT (HYbrid Single-Particle Lagrangian Integrated Trajectory) Model access via
8 NOAA ARL READY Website (<http://www.arl.noaa.gov/HYSPLIT.php>), NOAA Air
9 Resources Laboratory, College Park, MD)) to determine recent air mass history. Using
10 video, photos, and flight notes, clouds were also classified as either stratiform or
11 cumuliform. Stratiform clouds were present at 1-3 km altitude. With one exception (an
12 ARCTAS-B background case from 8 July 2008), the stratiform clouds were not present
13 below a strong temperature or moisture inversion. In our dataset, none of the biomass
14 burning cases were present below an inversion either; such inversions occurred only in
15 four of the clean background cases, indicating generally unimpeded aerosol mixing from
16 above and below for biomass burning clouds in these data. The cumuliform clouds were
17 also found between 1 and 3 km, and although they were less optically thick than the
18 stratiform clouds, optically thin ($\tau < 15$) and multi-layer clouds dominated all samples.
19 Across all clouds sampled during the four campaigns, there was substantial variation
20 between cloud properties (Table 7) and the physical locations of the clouds (Fig. 4). For
21 example, background clouds were primarily sampled over open-ocean and at higher
22 latitudes, whereas the smoky clouds were primarily sampled at lower latitudes over land.
23 For this reason, in addition to comparing median characteristics of all background and
24 clean cases, we also focus on a case study where multiple clean and smoky clouds were
25 observed under very similar meteorological and surface conditions (section 3.1).

26

27 **3 Results**

28 **3.1 Indirect effects of smoke in Arctic liquid phase clouds**

29 On 1 July 2008 during the ARCTAS-B campaign, a variety of small cumuliform clouds
30 were sampled during flight 18 over inland Saskatchewan, Canada. The physical

1 characteristics of the clouds were very similar (Table 8), being small (~0.7 km high, and
2 ~0.2-7 km wide) non-precipitating clouds present between 1680 and 2650 m altitude, and
3 far from any major temperature or water vapor inversions. All clouds were liquid phase,
4 with low median LWC values of 0.02 g m^{-3} (the implications of which is discussed
5 further down). All clouds had temperatures ranging from -0.1 to 3.1°C . All were
6 sampled within 97 km^2 and 5.2 hours of each other, during which time each cloud
7 experienced similar northeasterly wind direction.

8 Despite being exposed to similar meteorological and surface conditions, aerosol inputs to
9 these clouds ranged significantly, with average CH_3CN and PCASP equivalent particle
10 numbers ranging between 0.092-0.55 ppbv and $107\text{-}3001 \text{ cm}^{-3}$, respectively. The large
11 range in chemical properties was due to the aircraft track, which repeatedly covered areas
12 up- and downwind of local fresh smoke plumes from the Lake McKay fire. This fire is
13 comprehensively described in the combination of Cubison et al. (2011), Alvarado et al.
14 (2010), and Raatikainen et al. (2012).

15 In Fig. 3, we show that $\text{CO} < 500 \text{ ppbv}$ is strongly related to the smoke tracer CH_3CN
16 and that it shows no correlation to the fossil fuel combustion tracer dichloromethane
17 (CH_2Cl_2) (see Kondo et al., 2011 for further discussion on use of this tracer during
18 ARCTAS). Given that CO has both pollution and biomass burning sources, this finding
19 indicates smoke was the dominant aerosol contributor on that day, not pollution. Back
20 trajectories also support this conclusion (Alvarado et al., 2010). Of the clouds sampled
21 during this flight, two clouds met the classification criteria for being biomass burning
22 influenced, three were classified as intermediate, and two met the ARCTAS background
23 criteria.

24 As shown in Fig. 5, smoke is clearly correlated with reduced cloud droplet radius in the
25 seven clouds studied (with an average 59% reduction relative to background clouds,
26 Table 8). As expected, there was a concurrent increase in cloud droplet number (Fig. 5).
27 Based on this increase, we compute a combined median ACI of 0.05 (bootstrapped 95%
28 confidence interval 0.04-0.06) across all tracers shown in Fig. 5.

29 Although linear regressions were not used to derive ACIs, we plot them for each tracer in
30 Fig. 5 to show the degree of variation between individual tracer ACI values. Other

1 researchers have previously noted differences in calculated ACIs when these interactions
2 are computed from different tracers (e.g., McComiskey et al. (2009), Lihavainen et al.
3 (2010) and Zhao et al. (2012)), and these differences probably reflect a combination of
4 measurement error and how well a given tracer approximates the sub-population of
5 aerosols that are participating in cloud droplet activation (Lihavainen et al., 2010). As
6 plumes age, there may also be increasing uncertainty in biomass burning aerosol co-
7 location with gaseous tracers such as CO and CH₃CN, as these are subject to different
8 depositional processes (Hecobian et al., 2011). However, in this case the fires were
9 relatively fresh so this issue is unlikely to be an important source of uncertainty.

10 ACI estimates can also sometimes be influenced or even overwhelmed by systematic
11 differences in local meteorological conditions associated with cleaner versus more
12 polluted clouds (Hegg et al., 2007; Shao and Liu, 2006). For the case study, that
13 possibility is unlikely because of the relatively small area and time frame considered and
14 the similar meteorological conditions in which the clouds were sampled.

15 However, because case study smoky clouds had a combination of very low LWC, very
16 high aerosol concentrations from a fresh fire, and consequently, very small droplet sizes
17 (Fig. 6), it is likely that smoky case study clouds were less sensitive to further additions
18 of smoke aerosols than clouds with lower aerosol concentrations. Such non-linear
19 behavior is predicted when high CCN levels cause increased competition for water vapor,
20 which in turn decreases cloud supersaturation and reduces the tendency to form
21 additional drops (e.g., Moore et al. [2013]; Morales et al. [2011]; Morales and Nenes
22 [2010]). Additionally, possible enhanced entrainment of outside air in smoky clouds
23 compared to background clouds (Ackerman et al., 2004; Bretherton et al., 2007; Chen et
24 al., 2012; Lebsock et al., 2008) could enhance droplet evaporation and further reduce
25 ACI values from the expected adiabatic ACI maximum value at a given aerosol level.

26 Because in-situ ACI derivations assume linearity in the response of N_{liq} to BB_t , and such
27 as assumption does not hold well at high CCN levels, we would expect to derive lower
28 in-situ ACI estimates if clouds with very high CCN levels are included in the analysis
29 (Rosenfeld et al., 2014). That ACI values would increase to 0.08 (95% confidence
30 interval 0.05-0.12) if the two biomass burning clouds were excluded suggests that non-

1 linear processes could have affected the reduced ACI values in the case study. For
2 reference, at case study smoky CN_{PCASP} equivalent concentrations of $\sim 2,000-3,000 \text{ cm}^{-3}$,
3 modeled adiabatic ACI values were $\sim 0.06-0.16$ (Moore et al., 2013). The range in
4 modeled ACI values depended on factors such as cloud vertical velocity and CCN
5 hygroscopicity (the CCN spectrum). Given these model uncertainties and our estimated
6 case study ACI value, any potential effects of entrainment were not clearly noticeable in
7 our data.

8 For these reasons, although the 1 July 2008 case is in some ways ideal in that the clouds
9 were sampled in very similar environmental conditions, it is not necessarily
10 representative of typical cloud conditions in the Arctic. The clouds were present
11 relatively far south in the subarctic ($52-56^\circ\text{N}$) and were cumuliform compared to the
12 more dominant Arctic stratus type clouds. Moreover, the case study clouds were
13 subjected to fresh concentrated smoke rather than aged diluted smoke, as one would
14 expect at higher latitudes. Therefore, as explained above, we expect case study clouds
15 already affected by high smoke concentrations to have reduced sensitivity to additional
16 smoke, particularly given the low LWC of the case study clouds.

17 To assess the impact of smoke on liquid clouds more generally, we compared background
18 and biomass burning cloud properties sampled over the larger region shown in Fig. 4.
19 This more expansive set of clouds includes a broader range of high-latitude
20 meteorological conditions, making it more representative of overall conditions in the
21 Arctic region. However, the greater heterogeneity also makes trends in the data more
22 difficult to interpret, as we cannot describe in full detail the degree to which
23 meteorological influences affected each cloud given the limitations of the datasets.

24 Despite the uncertain meteorological influence, we see qualitatively similar trends to
25 those in the 1 July 2008 ARCTAS case study (Fig. 7). We find a $3.7 \mu\text{m}$ (42%) median
26 reduction in r_e between the smoky and background cases (Table 7). Concurrently,
27 median N_{liq} increased from 41 droplets cm^{-3} in background clouds to 338 droplets cm^{-3} in
28 smoky clouds. Within stratiform-only and cumuliform-only liquid clouds, groupings that
29 are somewhat more comparable meteorologically, the mean r_e differences are 2.5 and 6.4
30 μm ($n= 13$ and 14), respectively. However, the combined median ACI estimate from all

1 tracers shown in Fig. 7 is 0.16 (95% confidence interval 0.14-0.17). This value is three
2 times that of the case study, which is further evidence to suggest that cloud sensitivity to
3 aerosols in the case study was lowered by aerosol-driven adiabatic reductions in cloud
4 supersaturation (and possibly enhanced entrainment).

5 Observed smoke-driven reductions in liquid cloud droplet size and increases in cloud
6 droplet number in both the case study and the multi-campaign analysis are in line with
7 several other studies in the Arctic. Peng et al. (2002) found a similar difference in r_e of
8 4.8 μm to the multi-campaign analysis in two combined datasets in the Arctic (one of
9 which was the NRC FIRE.ACE dataset), in conditions where PCASP values were $>$ and
10 $<$ 300 particles cm^{-3} , although they did not specifically focus on biomass burning-related
11 samples. Tietze et al. (2011) also found significant changes in LWP, τ , and r_e using
12 remote sensing cloud observations combined with a modeled biomass burning tracer. In
13 contrast, Earle et al. (2011) did not see a reduction in r_e in biomass burning-influenced
14 clouds based on selected ISDAC samples. They attributed this finding to a combination
15 of meteorological and microphysical factors. It is possible that some of the differences
16 with our study are also caused by reduced contrast between selected clean and polluted
17 cases, as their cutoff for defining clean conditions was higher than ours, and they did not
18 include any samples that met our background criteria (which were only present during the
19 4 April 2008 ISDAC flight). Also note that the biomass burning-influenced cloud cases
20 assessed by Earle et al. (2011) did not overlap with the clouds assessed in this study.

21 As noted previously, because the aircraft could only sample transects of clouds, we had to
22 assume that the observed cloud phase was representative of the whole cloud. In the case
23 study, all clouds were sampled at temperatures $>$ 0 $^{\circ}\text{C}$, and this assumption holds well.

24 Where we expect this assumption to be most uncertain is in stratiform clouds in the
25 multi-campaign analysis, which might have different properties in far-off, non-sampled
26 portions. Uncertainties are also higher in clouds that were only transected horizontally,
27 because mixed phase clouds in the Arctic frequently have vertical layers of ice and liquid
28 particles (Morrison et al., 2012). We cannot fully rule out that non-sampled portions of
29 the clouds in the multi-campaign analysis contained ice particles, or that different vertical
30 layers had different r_e values. However, if the 6 ISDAC and FIRE.ACE background
31 clouds that were either stratiform or that contained only horizontal transects are excluded,

1 the results of the multi-campaign analysis are nearly the same (ACI = 0.15 and median
2 background cloud $r_e = 7.0$ vs. $7.6 \mu\text{m}$). Thus we do not believe that uncertainties in cloud
3 phase had a major impact on our results.

4 **3.2 Implications for radiation and precipitation**

5 Based on model output by McComiskey et al. (2008) (their Fig. 2a), we estimate that
6 given the case study median ACI value of 0.05, the smoke-derived cloud albedo effect on
7 summertime local shortwave radiative forcing could be between -2 to -4 W m^{-2} for
8 regions with surface albedo of ~ 0.15 . Typical shortwave spectrum broadband ($0.3\text{--}5.0$
9 μm) albedos over subarctic Canada range from $\sim 0.09\text{--}0.17$, compared to $\sim 0.23\text{--}0.71$ in the
10 winter (Davidson and Wang, 2005); thus, any local forcing in winter from smoke ACI
11 effects would likely be reduced, compared to the summer. The McComiskey et al.
12 (2008) output was also based on the assumption of homogeneous, unbroken clouds with
13 CCN concentrations of 600 cm^{-3} , a LWP of 50 g m^{-2} , and a cloud base height of 500 m .
14 Such surface albedo and cloud/aerosol conditions are similar to some of the summer
15 terrestrial conditions sampled over Canada during ARCTAS-B. The summer subarctic
16 biomass burning clouds we describe from ARCTAS-B CCN and LWP levels bracket the
17 model's assumptions, ranging between $1\text{--}94 \text{ g m}^{-2}$ and $68\text{--}6670 \text{ cm}^{-3}$, respectively.
18 However, cloud base heights were typically higher than the model-assumed 500 m , and
19 although unbroken clouds are frequently observed in the Arctic and subarctic, the ACI
20 value we use was determined from samples that included some clouds within broken
21 cloud systems, which may possibly have different microphysical responses to aerosols.
22 Periodic broken cloud conditions, cloud heterogeneity (McComiskey et al., 2008), and
23 the patchiness of smoke will all reduce the net cloud albedo radiative forcing over wider
24 spaces and times. Therefore, the -2 to -4 W m^{-2} range is only applicable in the subarctic
25 in some summertime conditions. Nonetheless, this estimate at least provides a rough
26 indication of how important these local effects might be during the most relevant time
27 periods (i.e., when burning is most likely to occur).

28 In contrast to the subarctic, in the Arctic high surface albedo will lessen the expected
29 impact of the cloud albedo effect. Although future sea ice losses and associated
30 reductions in surface albedo may affect the relative importance of the cloud albedo effect

1 on Arctic clouds, others (e.g., Garret et al. (2004)) have suggested that in the Arctic, a
2 more important impact of reduced cloud droplet size may be greater longwave opacity,
3 which can lead to enhanced snow melt. Relatedly, smaller droplets may affect cloud
4 lifetime either by extending it via reduced precipitation (the “second indirect effect”
5 (Ackerman et al., 2000; Albrecht, 1989)) or by reducing it via enhanced water vapor
6 competition and evaporation, as may have occurred in the case study.

7 Cloud droplet spectra from the 1 July 2008 ARCTAS case study clouds are shown in Fig.
8 6. Although sample size is small, the presence of smoke appears to narrow the droplet
9 spectra from a dispersion of 0.84 in background clouds to 0.55 in smoky clouds, as
10 calculated by the ratio between the standard deviation of the size distribution and the
11 mean droplet radius. This narrowing is likely to lessen the eventual probability of
12 precipitation (Tao et al., 2012), as it moves median droplet size further away from the 28
13 μm effective diameter threshold at which collision/coagulation processes are thought to
14 become efficient enough to induce precipitation (Rosenfeld et al., 2012).

15 Cloud droplet spectra from the multi-campaign clouds are shown for comparison in Fig.
16 8. There is not as obvious a narrowing of spectra as for the case study, but median droplet
17 concentrations in smoky clouds never reached above 28+ μm diameter, whereas median
18 droplet diameter in background clouds did reach above this point (Fig. 8). Also, small
19 droplet concentrations (those most susceptible to evaporation) increased in smoky
20 conditions, and rainfall was only noted in clean conditions, as shown in Fig. 8 by elevated
21 ($>0.1 \text{ cm}^{-3}$) cloud droplet concentrations with diameters $>50 \mu\text{m}$ (King et al., 2013).
22 Therefore, although clouds outside the case study suffer large uncertainties related to
23 their collection over heterogeneous conditions, their droplet distributions support the
24 hypothesis of smoke-induced reductions in drizzle.

25 **3.3 Interactions of background aerosols with dilute biomass burning** 26 **particles: a potential uncertainty in ACI values**

27 As mentioned previously, large numbers of nucleation- and Aitken-mode particles are
28 frequently observed in the spring and summer Arctic and subarctic (Engvall et al., 2008;
29 Leck and Bigg, 1999; Ström et al., 2009; Zhao and Garrett, 2015). These particles are
30 thought to have a marine origin via some combination of new particle formation from

1 marine gases (Allan et al., 2015; Leaitch et al., 2013; O'Dowd et al., 2010; Tunved et al.,
2 2013) and direct oceanic nanogel emissions (Heintzenberg et al., 2006; Karl et al., 2012,
3 2013; Leck and Bigg, 1999; Orellana et al., 2011). Chemical data from the ARCTAS
4 dataset also show the presence of numerous small particles with a natural background
5 source (Fig. 9).

6 Previous studies also suggest that the small particles can condense upon larger particles
7 (e.g., smoke) when such particles are present (Engvall et al., 2008; Leaitch et al., 2013;
8 Tunved et al., 2013). This coagulation process may explain why Arctic smoke aerosols
9 have been shown to sometimes contain organic components likely derived from smaller,
10 non-biomass burning particles mixed with sulphates and marine particles (Earle et al.,
11 2011; Zelenyuk et al., 2010). To get some idea of how important the background particles
12 may be, we estimated the maximum mean aerosol volume change that would occur if
13 high concentrations of small background aerosols were to mix with and condense upon
14 diluted smoke particles. Concentrations of background particles were estimated at 5000
15 cm^{-3} (based on high-end values observed in Fig. 9 and at another Arctic site (Ström et al.,
16 2009)). Diluted smoke concentrations were estimated at 450 particles cm^{-3} (low-end
17 values from Fig. 9). Volumes were calculated from the size ranges observed in ARCTAS
18 background and smoky aerosols (see Appendix A for details). In this hypothetical
19 scenario, we estimate that background aerosols could increase dilute smoke aerosol
20 volume by up to 2-15%, although volume increases are likely substantially less in most
21 air masses.

22 Interestingly, the small Arctic marine particles appear to be fairly hygroscopic (Latham et
23 al., 2013; Lawler et al., 2014; Zhou et al., 2001), and they can be surface active
24 (Lohmann and Leck, 2005). One study using ARCTAS data showed that background
25 aerosol values of the hygroscopicity parameter, κ , were on average nearly two times
26 higher than average smoke κ values (0.32 ± 0.21 vs. 0.18 ± 0.13 , respectively), although
27 there was a high degree of variability and overlap in the κ values (Latham et al., 2013).
28 Previous studies also suggest that volume increases alone might affect Arctic particle
29 hygroscopicity, independent of chemistry (Moore et al., 2011). Given this information,
30 we cannot rule out that upon condensation, the small background particles might act as
31 surfactants or otherwise modify smoke CCN characteristics, causing deviations from the

1 ACI value as derived in section 3.1 at low smoke concentrations. This hypothesis is
2 difficult to test because, excepting three intermediate instances in the case study, the data
3 presented in Section 3.2 only included background and high smoke conditions.

4 However, the nucleation- and Aitken-mode background particles are not ubiquitous
5 throughout the year. They tend to accumulate mainly in the spring and summer, which is
6 thought to be due to a combination of three factors: 1) there is more sunlight available for
7 the photochemical reactions key to new particle formation (Engvall et al., 2008; Tunved
8 et al., 2013), 2) reduced sea ice and enhanced primary production likely lead to greater
9 emissions of marine precursor gases and nanogels (Leaitch et al., 2013; O’Dowd et al.,
10 2010; Tunved et al., 2013), and 3) during Arctic summer there tend to be fewer larger
11 particles such as smoke for these small particles to coagulate and condense upon.

12 However, Arctic summertime smoke events do occur (e.g., Fuelberg et al. (2010);
13 Iziomon et al. (2006)) and may be increasing (Moritz et al., 2012). In the subarctic,
14 wildfires peak in the summer (Giglio et al., 2006). Thus, although the influence of the
15 small background particles on subarctic and Arctic smoke ACI values is probably minor,
16 deviations from the linear ACI expectations derived here might occur during dilute
17 summertime Arctic smoke events and in subarctic locations: for example when smoke is
18 diluted over or near marine environments.

19

20 **4 Discussion and Conclusions**

21 The challenge of separating the influence of meteorology and aerosol indirect effects on
22 clouds introduces relatively large uncertainty in our understanding of how smoke impacts
23 clouds. Using in situ aircraft data, we quantified these impacts in both a subarctic
24 cumulus cloud case study and in a multi-campaign data assessment of clouds north of
25 50°N. The multi-campaign assessment suggests an ACI value of 0.16 (95% confidence
26 interval 0.10-0.13), which is on the high end of previous satellite-based assessments
27 (0.04-0.11) (Tietze et al., 2011). Given a known low bias in remote-sensing-derived
28 estimates of ACI (e.g., McComiskey et al. (2012)), our findings suggest that smoke-
29 derived increases in cloud albedo may be higher than previously derived in the region.
30 We reduced confounding meteorological effects by including data from as wide a

1 geographic region as possible, applying very stringent conditions to identify clean and
2 smoky clouds, and reducing the impact of outliers on ACI derivations by using the
3 Kendall robust line-fit method instead of normal linear regressions. However it is
4 important to note that meteorological effects are still imperfectly constrained in this
5 assessment due to inherent limitations in the in situ dataset size and content.

6 For comparison to the multi-campaign analysis, we also analyzed the 1 July 2008
7 ARCTAS case in the subarctic, where multiple clean and smoky clouds were found under
8 similar meteorological conditions. The case study smoke cases had a combination of low
9 cloud LWC, high in-plume aerosol concentrations, and very small cloud droplets. From
10 these samples we derived an ACI estimate of 0.05 (95% confidence interval 0.04-0.06),
11 which is smaller than that of the multi-campaign analysis. Based on theory (e.g., Moore
12 et al. (2013)), as the number of smoke CCN increases (through some combination of
13 enhanced aerosol number and/or increased hygroscopicity for existing particles), there is
14 greater water vapor competition. This competition makes supersaturation development
15 and cloud droplet activation increasingly difficult, which would reduce ACI values.
16 Therefore, we speculate that the 0.05 ACI case study value falls at the low-end of typical
17 smoke ACI values for the larger subarctic/Arctic region. Reductions in droplet activation
18 and potential enhanced evaporation would also limit the maximum magnitude of smoke
19 cloud albedo effects.

20 Based on a previous model study by McComiskey et al. (2008), the ACI value of 0.05
21 from the case study suggests that smoke may reduce local summertime radiative flux via
22 the cloud albedo effect by between 2-4 W m⁻² or more under low and homogeneous cloud
23 cover conditions in the subarctic. At higher latitudes where surface albedo is already
24 high, the impact on radiative flux is likely to be smaller. In those regions, a more
25 important effect of smoke might be its inhibition of precipitation and cloud lifetime
26 effect, as evidenced by the observed reductions in cloud droplet radius of ~50% in both
27 the case study and the multi-campaign assessment.

28 Smaller cloud droplets can have various consequences. Smoke-driven reductions or
29 delays in precipitation may affect the distribution of aerosol and moisture deposition.
30 Longer cloud lifetime could impact not only Arctic albedo but also longwave radiation

1 (Stone, 1997), and previous studies suggest that even small changes in the above
2 parameters may affect sensitive Arctic sea ice (Kay et al., 2008; Kay and Gettelman,
3 2009; Lubin and Vogelmann, 2006; Vavrus et al., 2010). Additionally, changes in cloud
4 cover might also have indirect effects on ocean photosynthesis and biogeochemistry
5 (Bélanger et al., 2013). It is our hope that the improved quantification of smoke-derived
6 ACI values will help quantify these impacts in future model studies.

7 One obvious limitation of our study is that we do not address the impacts of smoke on
8 existing mixed and ice phase clouds. Additionally, we cannot account for the ways in
9 which smoke might have affected sample phase. For example, ice nuclei presence might
10 facilitate the conversion of an otherwise liquid phase cloud into a mixed phase cloud that
11 was excluded in this assessment. Alternatively, we could have included liquid clouds in
12 our assessment that might otherwise have been present as mixed or ice phase clouds if
13 not for the inhibition of freezing by soluble smoke compounds via the Raoult effect
14 (discussed in Tao et al. (2012)).

15 Finally, we have presented evidence to suggest that coagulation of the numerous
16 nucleation- and Aitken-mode background particles frequently present in clean
17 summertime Arctic air masses might increase the volume of diluted smoke aerosols by
18 up to 2-15%. Previous studies suggest that such interactions with background particles
19 may increase smoke aerosol hygroscopicity, which in turn could cause deviations from
20 the ACI value derived here. Future remote sensing or ground-based analyses may be able
21 to more completely address the different impacts of dilute vs. concentrated smoke
22 aerosols in Arctic clouds.

23

24 **Appendix A: Calculations for maximum potential contribution of** 25 **background aerosol to diluted smoke aerosol volume**

26 We first estimate the volume of smoke particles at dilute concentrations of 450 particles
27 cm^{-3} . Arctic/subarctic smoke aerosol size distributions were taken from Kondo et al.
28 (2011) and Sakamoto et al. (2015), where lognormal aerosol size distributions were
29 characterized by geometric mean diameters of 224 ± 14 nm and 230 nm and geometric
30 standard deviations of 1.33 ± 0.05 and 1.5, respectively. From the corresponding size

1 distributions, we estimate smoke aerosol volumes of $\sim 2.9\text{-}6.0 \mu\text{m}^3$ per cm^{-3} of air at
2 smoke concentrations of 450 cm^{-3} .

3 The degree to which aerosol properties can be affected by the collection of Arctic
4 nucleation- and Aitken-mode background particles onto larger smoke and pollution
5 particles also depends in part on the size ranges and concentrations of the background
6 particles. These can be quite variable (Engvall et al., 2008) (also see Fig. A1). To
7 estimate average background concentrations, we use the observed geometric mean ratio
8 range in 6-year Svalbard summertime data (Engvall et al., 2008), which indicated that
9 Aitken-mode particle concentrations were $\sim 1.5\text{-}3$ times greater than those of
10 accumulation-mode particles. Given this range in ratios, we would expect background
11 particle concentrations to be $\sim 675\text{-}1350 \text{ cm}^{-3}$ at smoke concentrations of 450 cm^{-3} . We
12 then combine the expected small background aerosol concentrations with ARCTAS
13 background aerosol spectra from events from 12 April, 10 July, and 13 July 2008 (Fig.
14 A1) for particles $< 80 \text{ nm}$ in diameter. Based on these values, small background aerosol
15 volume is estimated at $0.012\text{-}0.114 \mu\text{m}^3 \text{ cm}^{-3}$. A comparison of this volume with the
16 previously estimated smoke aerosol volume suggests that background aerosols could
17 contribute only $\sim 0.2\text{-}4\%$ of total diluted smoke aerosol volume in average summertime
18 conditions. This estimate does not account the fact that all else being equal, small
19 particles are usually more likely to coagulate onto the largest sized particles (Seinfeld and
20 Pandis, 1998), which would reduce the contribution to average particle volume even
21 further.

22 Alternatively, we can estimate what the background aerosol volume might be if particle
23 concentrations were as high as 5000 cm^{-3} . Although such events are not common in the
24 Arctic and subarctic, similar high-end concentrations of background particles are
25 observed in Figure 9 and have been observed elsewhere in the Arctic as well (Ström et
26 al., 2009). Again assuming the same range of particle size distributions observed in Fig.
27 A1, the small background aerosol volume at $5000 \text{ particles cm}^{-3}$ is estimated to be
28 between $0.092\text{-}0.422 \mu\text{m}^3$ per cm^{-3} of air. Thus, in this case background aerosols could
29 add at most $2\text{-}15\%$ of total aerosol volume in diluted smoke with concentrations of 450
30 particles cm^{-3} .

1

2 **Acknowledgements**

3 The authors would like to thank A. Aknan, B. Anderson, E. Apel, G. Chen, M. Couture,
4 T. Garrett, K.B. Huebert, A. Khain, A. Korolev, T. Lathem, P. Lawson, R. Leitch, J.
5 Limbacher, J. Nelson, M. Pinsky, W. Ridgeway, A. Rangno, S. Williams, S. Woods, and
6 Y. Yang for data and/or advice or help with various aspects of this project, and all others
7 who were involved in collecting and funding the collection of the datasets we have used.
8 We acknowledge the Atmospheric Radiation Measurement (ARM) Program sponsored
9 by the U.S. Department of Energy, Office of Science, Office of Biological and
10 Environmental Research, Climate and Environmental Sciences Division for providing the
11 ISDAC dataset. The authors also gratefully acknowledge the NOAA Air Resources
12 Laboratory (ARL) for the provision of the HYSPLIT transport and dispersion model
13 and/or READY website (<http://www.ready.noaa.gov>) used in this publication. Plots were
14 made with Ocean Data View (Schlitzer, R., Ocean Data View, <http://odv.awi.de>, 2015)
15 and R (R Core Team, 2013). CH₃CN measurements were supported by the Austrian
16 Federal Ministry for Transport, Innovation and Technology (bmvit) through the Austrian
17 Space Applications Programme (ASAP) of the Austrian Research Promotion Agency
18 (FFG). T. Mikoviny is acknowledged for his support with the CH₃CN data acquisition
19 and analysis. LMZ's funding for this study was provided by an appointment to the NASA
20 Postdoctoral Program at Goddard Space Flight Center, administered by Oak Ridge
21 Associated Universities through a contract with NASA. MJC and JLJ were supported by
22 NASA NNX12AC03G and NNX15AH33A.

1 **References**

- 2 Ackerman, A. S., Toon, O. B., Stevens, D. E., Heymsfield, A. J., Ramanathan, V. and
3 Welton, E. J.: Reduction of Tropical Cloudiness by Soot, *Science*, 288(5468), 1042–
4 1047, doi:10.1126/science.288.5468.1042, 2000.
- 5 Ackerman, A. S., Kirkpatrick, M. P., Stevens, D. E. and Toon, O. B.: The impact of
6 humidity above stratiform clouds on indirect aerosol climate forcing, *Nature*, 432(7020),
7 1014–1017, doi:10.1038/nature03174, 2004.
- 8 Albrecht, B. A.: Aerosols, Cloud Microphysics, and Fractional Cloudiness, *Science*,
9 245(4923), 1227–1230, doi:10.1126/science.245.4923.1227, 1989.
- 10 Allan, J. D., Williams, P. I., Najera, J., Whitehead, J. D., Flynn, M. J., Taylor, J. W.,
11 Liu, D., Darbyshire, E., Carpenter, L. J., Chance, R., Andrews, S. J., Hackenberg, S. C.,
12 and McFiggans, G.: Iodine observed in new particle formation events in the Arctic
13 atmosphere during ACCACIA, *Atmos. Chem. Phys.*, 15, 5599-5609, doi:10.5194/acp-15-
14 5599-2015, 2015.
- 15 Alvarado, M. J., Logan, J. A., Mao, J., Apel, E., Riemer, D., Blake, D., Cohen, R. C.,
16 Min, K.-E., Perring, A. E., Browne, E. C., Wooldridge, P. J., Diskin, G. S., Sachse, G.
17 W., Fuelberg, H., Sessions, W. R., Harrigan, D. L., Huey, G., Liao, J., Case-Hanks, A.,
18 Jimenez, J. L., Cubison, M. J., Vay, S. A., Weinheimer, A. J., Knapp, D. J., Montzka, D.
19 D., Flocke, F. M., Pollack, I. B., Wennberg, P. O., Kurten, A., Crouse, J., Clair, J. M. S.,
20 Wisthaler, A., Mikoviny, T., Yantosca, R. M., Carouge, C. C. and Le Sager, P.: Nitrogen
21 oxides and PAN in plumes from boreal fires during ARCTAS-B and their impact on
22 ozone: an integrated analysis of aircraft and satellite observations, *Atmos Chem Phys*,
23 10(20), 9739–9760, doi:10.5194/acp-10-9739-2010, 2010.
- 24 Avramov, A., Ackerman, A. S., Fridlind, A. M., van Dierenhoven, B., Botta, G., Aydin,
25 K., Verlinde, J., Korolev, A. V., Strapp, J. W., McFarquhar, G. M., Jackson, R., Brooks,
26 S. D., Glen, A. and Wolde, M.: Toward ice formation closure in Arctic mixed-phase
27 boundary layer clouds during ISDAC, *J. Geophys. Res. Atmospheres*, 116(D1), D00T08,
28 doi:10.1029/2011JD015910, 2011.

1 Balshi, M. S., Mcguire, A. D., Duffy, P., Flannigan, M., Kicklighter, D. W. and Melillo,
2 J.: Vulnerability of carbon storage in North American boreal forests to wildfires during
3 the 21st century, *Glob. Change Biol.*, 15(6), 1491–1510, doi:10.1111/j.1365-
4 2486.2009.01877.x, 2009.

5 Baum, B. A., Menzel, W. P., Frey, R. A., Tobin, D. C., Holz, R. E., Ackerman, S. A.,
6 Heidinger, A. K. and Yang, P.: MODIS Cloud-Top Property Refinements for Collection
7 6, *J. Appl. Meteorol. Climatol.*, 51(6), 1145–1163, doi:10.1175/JAMC-D-11-0203.1,
8 2012.

9 Baumgardner, D., Jonsson, H., Dawson, W., O'Connor, D. and Newton, R.: The cloud,
10 aerosol and precipitation spectrometer: a new instrument for cloud investigations,
11 *Atmospheric Res.*, 59–60, 251–264, doi:10.1016/S0169-8095(01)00119-3, 2001.

12 Bélanger, S., Babin, M. and Tremblay, J.-É.: Increasing cloudiness in Arctic damps the
13 increase in phytoplankton primary production due to sea ice receding, *Biogeosciences*,
14 10(6), 4087–4101, doi:10.5194/bg-10-4087-2013, 2013.

15 Bian, H., Colarco, P. R., Chin, M., Chen, G., Rodriguez, J. M., Liang, Q., Blake, D., Chu,
16 D. A., da Silva, A., Darmenov, A. S., Diskin, G., Fuelberg, H. E., Huey, G., Kondo, Y.,
17 Nielsen, J. E., Pan, X. and Wisthaler, A.: Source attributions of pollution to the Western
18 Arctic during the NASA ARCTAS field campaign, *Atmos Chem Phys*, 13(9), 4707–
19 4721, doi:10.5194/acp-13-4707-2013, 2013.

20 Bodhaine, B. A., Harris, J. M. and Herbert, G. A.: Aerosol light scattering and
21 condensation nuclei measurements at Barrow, Alaska, *Atmospheric Environ.* 1967, 15(8),
22 1375–1389, doi:10.1016/0004-6981(81)90344-9, 1981.

23 Bourgeois, Q. and Bey, I.: Pollution transport efficiency toward the Arctic: Sensitivity to
24 aerosol scavenging and source regions, *J. Geophys. Res. Atmospheres*, 116(D8), n/a–n/a,
25 doi:10.1029/2010JD015096, 2011.

26 Bretherton, C. S., Blossey, P. N. and Uchida, J.: Cloud droplet sedimentation,
27 entrainment efficiency, and subtropical stratocumulus albedo, *Geophys. Res. Lett.*, 34(3),
28 L03813, doi:10.1029/2006GL027648, 2007.

1 Brock, C. A., Cozic, J., Bahreini, R., Froyd, K. D., Middlebrook, A. M.,
2 McComiskey, A., Brioude, J., Cooper, O. R., Stohl, A., Aikin, K. C., de Gouw, J. A.,
3 Fahey, D. W., Ferrare, R. A., Gao, R.-S., Gore, W., Holloway, J. S., Hübner, G.,
4 Jefferson, A., Lack, D. A., Lance, S., Moore, R. H., Murphy, D. M., Nenes, A.,
5 Novelli, P. C., Nowak, J. B., Ogren, J. A., Peischl, J., Pierce, R. B., Pilewskie, P.,
6 Quinn, P. K., Ryerson, T. B., Schmidt, K. S., Schwarz, J. P., Sodemann, H.,
7 Spackman, J. R., Stark, H., Thomson, D. S., Thornberry, T., Veres, P., Watts, L. A.,
8 Warneke, C., and Wollny, A. G.: Characteristics, sources, and transport of aerosols
9 measured in spring 2008 during the aerosol, radiation, and cloud processes affecting
10 Arctic Climate (ARCPAC) Project, *Atmos. Chem. Phys.*, 11, 2423-2453,
11 doi:10.5194/acp-11-2423-2011, 2011.

12 Cai, Y., Montague, D. C., Mooiweer-Bryan, W. and Deshler, T.: Performance
13 characteristics of the ultra high sensitivity aerosol spectrometer for particles between 55
14 and 800 nm: Laboratory and field studies, *J. Aerosol Sci.*, 39(9), 759–769,
15 doi:10.1016/j.jaerosci.2008.04.007, 2008.

16 Chen, Y.-C., Christensen, M. W., Xue, L., Sorooshian, A., Stephens, G. L., Rasmussen,
17 R. M. and Seinfeld, J. H.: Occurrence of lower cloud albedo in ship tracks, *Atmos Chem*
18 *Phys*, 12(17), 8223–8235, doi:10.5194/acp-12-8223-2012, 2012.

19 Colman, J. J., Swanson, A. L., Meinardi, S., Sive, B. C., Blake, D. R. and Rowland, F. S.:
20 Description of the Analysis of a Wide Range of Volatile Organic Compounds in Whole
21 Air Samples Collected during PEM-Tropics A and B, *Anal. Chem.*, 73(15), 3723–3731,
22 doi:10.1021/ac010027g, 2001.

23 Corr, C. A., Hall, S. R., Ullmann, K., Anderson, B. E., Beyersdorf, A. J., Thornhill, K. L.,
24 Cubison, M. J., Jimenez, J. L., Wisthaler, A. and Dibb, J. E.: Spectral absorption of
25 biomass burning aerosol determined from retrieved single scattering albedo during
26 ARCTAS, *Atmos Chem Phys*, 12(21), 10505–10518, doi:10.5194/acp-12-10505-2012,
27 2012.

28 Costantino, L. and Bréon, F.-M.: Analysis of aerosol-cloud interaction from multi-sensor
29 satellite observations, *Geophys. Res. Lett.*, 37(11), L11801, doi:10.1029/2009GL041828,
30 2010.

1 Cubison, M. J., Ortega, A. M., Hayes, P. L., Farmer, D. K., Day, D., Lechner, M. J.,
2 Brune, W. H., Apel, E., Diskin, G. S., Fisher, J. A., Fuelberg, H. E., Hecobian, A.,
3 Knapp, D. J., Mikoviny, T., Riemer, D., Sachse, G. W., Sessions, W., Weber, R. J.,
4 Weinheimer, A. J., Wisthaler, A. and Jimenez, J. L.: Effects of aging on organic aerosol
5 from open biomass burning smoke in aircraft and laboratory studies, *Atmos Chem Phys*,
6 11(23), 12049–12064, doi:10.5194/acp-11-12049-2011, 2011.

7 Curry, J. A., Hobbs, P. V., King, M. D., Randall, D. A., Minnis, P., Isaac, G. A., Pinto, J.
8 O., Uttal, T., Bucholtz, A., Cripe, D. G., Gerber, H., Fairall, C. W., Garrett, T. J., Hudson,
9 J., Intrieri, J. M., Jakob, C., Jensen, T., Lawson, P., Marcotte, D., Nguyen, L., Pilewskie,
10 P., Rangno, A., Rogers, D. C., Strawbridge, K. B., Valero, F. P. J., Williams, A. G. and
11 Wylie, D.: FIRE Arctic Clouds Experiment, *Bull. Am. Meteorol. Soc.*, 81(1), 5–29,
12 doi:10.1175/1520-0477(2000)081<0005:FACE>2.3.CO;2, 2000.

13 Davidson, A. and Wang, S.: Spatiotemporal variations in land surface albedo across
14 Canada from MODIS observations, *Can. J. Remote Sens.*, 31(5), 377–390,
15 doi:10.5589/m05-021, 2005.

16 DeCarlo, P. F., Dunlea, E. J., Kimmel, J. R., Aiken, A. C., Sueper, D., Crouse, J.,
17 Wennberg, P. O., Emmons, L., Shinozuka, Y., Clarke, A., Zhou, J., Tomlinson, J.,
18 Collins, D. R., Knapp, D., Weinheimer, A. J., Montzka, D. D., Campos, T. and Jimenez,
19 J. L.: Fast airborne aerosol size and chemistry measurements above Mexico City and
20 Central Mexico during the MILAGRO campaign, *Atmos Chem Phys*, 8(14), 4027–4048,
21 doi:10.5194/acp-8-4027-2008, 2008.

22 Duong, H. T., Sorooshian, A. and Feingold, G.: Investigating potential biases in observed
23 and modeled metrics of aerosol-cloud-precipitation interactions, *Atmos Chem Phys*,
24 11(9), 4027–4037, doi:10.5194/acp-11-4027-2011, 2011.

25 Earle, M. E., Liu, P. S. K., Strapp, J. W., Zelenyuk, A., Imre, D., McFarquhar, G. M.,
26 Shantz, N. C. and Leitch, W. R.: Factors influencing the microphysics and radiative
27 properties of liquid-dominated Arctic clouds: Insight from observations of aerosol and
28 clouds during ISDAC, *J. Geophys. Res.*, 116(D1), D00T09, doi:10.1029/2011JD015887,
29 2011.

1 Engvall, A.-C., Krejci, R., Ström, J., Treffeisen, R., Scheele, R., Hermansen, O. and
2 Paatero, J.: Changes in aerosol properties during spring-summer period in the Arctic
3 troposphere, *Atmos Chem Phys*, 8(3), 445–462, doi:10.5194/acp-8-445-2008, 2008.

4 Feingold, G., Eberhard, W. L., Veron, D. E. and Previdi, M.: First measurements of the
5 Twomey indirect effect using ground-based remote sensors, *Geophys. Res. Lett.*, 30(6),
6 1287, doi:10.1029/2002GL016633, 2003.

7 Feingold, G., Remer, L. A., Ramaprasad, J. and Kaufman, Y. J.: Analysis of smoke
8 impact on clouds in Brazilian biomass burning regions: An extension of Twomey’s
9 approach, *J. Geophys. Res. Atmospheres*, 106(D19), 22907–22922,
10 doi:10.1029/2001JD000732, 2001.

11 Fisher, J. A., Jacob, D. J., Purdy, M. T., Kopacz, M., Le Sager, P., Carouge, C., Holmes,
12 C. D., Yantosca, R. M., Batchelor, R. L., Strong, K., Diskin, G. S., Fuelberg, H. E.,
13 Holloway, J. S., Hyer, E. J., McMillan, W. W., Warner, J., Streets, D. G., Zhang, Q.,
14 Wang, Y. and Wu, S.: Source attribution and interannual variability of Arctic pollution in
15 spring constrained by aircraft (ARCTAS, ARCPAC) and satellite (AIRS) observations of
16 carbon monoxide, *Atmos Chem Phys*, 10(3), 977–996, doi:10.5194/acp-10-977-2010,
17 2010.

18 Flannigan, M. D., Krawchuk, M. A., de Groot, W. J., Wotton, B. M. and Gowman, L. M.:
19 Implications of changing climate for global wildland fire, *Int. J. Wildland Fire*, 18(5),
20 483–507, 2009.

21 Fridlind, A. M., van Dierenhoven, B., Ackerman, A. S., Avramov, A., Mrowiec, A.,
22 Morrison, H., Zuidema, P. and Shupe, M. D.: A FIRE-ACE/SHEBA Case Study of
23 Mixed-Phase Arctic Boundary Layer Clouds: Entrainment Rate Limitations on Rapid
24 Primary Ice Nucleation Processes, *J. Atmospheric Sci.*, 69(1), 365–389,
25 doi:10.1175/JAS-D-11-052.1, 2012.

26 Fuelberg, H. E., Harrigan, D. L. and Sessions, W.: A meteorological overview of the
27 ARCTAS 2008 mission, *Atmos Chem Phys*, 10(2), 817–842, doi:10.5194/acp-10-817-
28 2010, 2010.

1 Garrett, T. J. and Hobbs, P. V.: Calibration of liquid water probes from the University of
2 Washington's CV-580 aircraft at the Canadian NRC wind tunnel, in Rep. Cloud and
3 Aerosol Research Group, p. 20 pp., Dep. of Atmos. Sci, Univ. of Washington, Seattle.,
4 1999.

5 Garrett, T. J., Zhao, C., Dong, X., Mace, G. G. and Hobbs, P. V.: Effects of varying
6 aerosol regimes on low-level Arctic stratus, *Geophys. Res. Lett.*, 31(17), L17105,
7 doi:10.1029/2004GL019928, 2004.

8 Giglio, L., Csizsar, I. and Justice, C. O.: Global distribution and seasonality of active fires
9 as observed with the Terra and Aqua Moderate Resolution Imaging Spectroradiometer
10 (MODIS) sensors, *J. Geophys. Res. Biogeosciences*, 111(G2), G02016,
11 doi:10.1029/2005JG000142, 2006.

12 De Gouw, J. A., Warneke, C., Parrish, D. D., Holloway, J. S., Trainer, M. and
13 Fehsenfeld, F. C.: Emission sources and ocean uptake of acetonitrile (CH₃CN) in the
14 atmosphere, *J. Geophys. Res. Atmospheres*, 108(D11), 4329,
15 doi:10.1029/2002JD002897, 2003.

16 Hansen, J. E. and Travis, L. D.: Light scattering in planetary atmospheres, *Space Sci.*
17 *Rev.*, 16(4), 527–610, doi:10.1007/BF00168069, 1974.

18 Hecobian, A., Liu, Z., Hennigan, C. J., Huey, L. G., Jimenez, J. L., Cubison, M. J., Vay,
19 S., Diskin, G. S., Sachse, G. W., Wisthaler, A., Mikoviny, T., Weinheimer, A. J., Liao, J.,
20 Knapp, D. J., Wennberg, P. O., Kürten, A., Crouse, J. D., Clair, J. S., Wang, Y. and
21 Weber, R. J.: Comparison of chemical characteristics of 495 biomass burning plumes
22 intercepted by the NASA DC-8 aircraft during the ARCTAS/CARB-2008 field
23 campaign, *Atmos Chem Phys*, 11(24), 13325–13337, doi:10.5194/acp-11-13325-2011,
24 2011.

25 Hegg, D. A., Nielsen, K., Covert, D. S., Jonsson, H. H. and Durkee, P. A.: Factors
26 influencing the mesoscale variations in marine stratocumulus albedo, *Tellus B*, 59(1),
27 doi:10.3402/tellusb.v59i1.16970, 2007.

1 Hegg, D. A., Warren, S. G., Grenfell, T. C., Doherty, S. J., Larson, T. V. and Clarke, A.
2 D.: Source Attribution of Black Carbon in Arctic Snow, *Environ. Sci. Technol.*, 43(11),
3 4016–4021, doi:10.1021/es803623f, 2009.

4 Hegg, D. A., Warren, S. G., Grenfell, T. C., Sarah J Doherty and Clarke, A. D.: Sources
5 of light-absorbing aerosol in arctic snow and their seasonal variation, *Atmos Chem Phys*,
6 10(22), 10923–10938, doi:10.5194/acp-10-10923-2010, 2010.

7 Heintzenberg, J., Leck, C., Birmili, W., Wehner, B., Tjernström, M. and Wiedensohler,
8 A.: Aerosol number–size distributions during clear and fog periods in the summer high
9 Arctic: 1991, 1996 and 2001, *Tellus B*, 58(1), 41–50, doi:10.1111/j.1600-
10 0889.2005.00171.x, 2006.

11 Howell, S. G., Clarke, A. D., Freitag, S., McNaughton, C. S., Kapustin, V., Brekovskikh,
12 V., Jimenez, J.-L. and Cubison, M. J.: An airborne assessment of atmospheric particulate
13 emissions from the processing of Athabasca oil sands, *Atmos Chem Phys*, 14(10), 5073–
14 5087, doi:10.5194/acp-14-5073-2014, 2014.

15 Huffman, J., Jayne, J., Drewnick, F., Aiken, A., Onasch, T., Worsnop, D. and Jimenez, J.:
16 Design, Modeling, Optimization, and Experimental Tests of a Particle Beam Width Probe
17 for the Aerodyne Aerosol Mass Spectrometer, *Aerosol Sci. Technol.*, 39(12), 1143–1163,
18 doi:10.1080/02786820500423782, 2005.

19 Intrieri, J. M., Shupe, M. D., Uttal, T. and McCarty, B. J.: An annual cycle of Arctic
20 cloud characteristics observed by radar and lidar at SHEBA, *J. Geophys. Res. Oceans*,
21 107(C10), SHE 5–1, doi:10.1029/2000JC000423, 2002.

22 Iziomon, M. G., Lohmann, U. and Quinn, P. K.: Summertime pollution events in the
23 Arctic and potential implications, *J. Geophys. Res.*, 111(D12), D12206,
24 doi:10.1029/2005JD006223, 2006.

25 Jackson, R. C., McFarquhar, G. M., Korolev, A. V., Earle, M. E., Liu, P. S. K., Lawson,
26 R. P., Brooks, S., Wolde, M., Laskin, A. and Freer, M.: The dependence of ice
27 microphysics on aerosol concentration in arctic mixed-phase stratus clouds during
28 ISDAC and M-PACE, *J. Geophys. Res.*, 117(D15), D15207, doi:10.1029/2012JD017668,
29 2012.

1 Jacob, D. J., Crawford, J. H., Maring, H., Clarke, A. D., Dibb, J. E., Emmons, L. K.,
2 Ferrare, R. A., Hostetler, C. A., Russell, P. B., Singh, H. B., Thompson, A. M., Shaw, G.
3 E., McCauley, E., Pederson, J. R. and Fisher, J. A.: The Arctic Research of the
4 Composition of the Troposphere from Aircraft and Satellites (ARCTAS) mission: design,
5 execution, and first results, *Atmos Chem Phys*, 10(11), 5191–5212, doi:10.5194/acp-10-
6 5191-2010, 2010.

7 Jouan, C., Girard, E., Pelon, J., Gultepe, I., Delanoë, J. and Blanchet, J.-P.:
8 Characterization of Arctic ice cloud properties observed during ISDAC, *J. Geophys. Res.*
9 *Atmospheres*, 117(D23), D23207, doi:10.1029/2012JD017889, 2012.

10 Karl, M., Leck, C., Gross, A., and Pirjola, L.: A study of new particle formation in the
11 marine boundary layer over the central Arctic ocean using a flexible multicomponent
12 aerosol dynamic model, *Tellus*, 64B, 17158, doi:10.3402/tellusb.v64i0.17158, 2012.

13 Karl, M., Leck, C., Coz, E. and Heintzenberg, J.: Marine nanogels as a source of
14 atmospheric nanoparticles in the high Arctic, *Geophys. Res. Lett.*, 40(14), 3738–3743,
15 doi:10.1002/grl.50661, 2013.

16 Kay, J. E. and Gettelman, A.: Cloud influence on and response to seasonal Arctic sea ice
17 loss, *J. Geophys. Res.*, 114, D18204, doi:10.1029/2009JD011773, 2009.

18 Kay, J. E., Ecuyer, T. L., Gettelman, A., Stephens, G., and O’Dell, C.: The contribution of
19 cloud and radiation anomalies to the 2007 Arctic sea ice extent minimum, *Geophys. Res.*
20 *Let.*, 35, L08503, doi:10.1029/2008GL033451, 2008.

21 King, N. J., Bower, K. N., Crosier, J. and Crawford, I.: Evaluating MODIS cloud
22 retrievals with in situ observations from VOCALS-REx, *Atmos Chem Phys*, 13(1), 191–
23 209, doi:10.5194/acp-13-191-2013, 2013.

24 Kondo, Y., Matsui, H., Moteki, N., Sahu, L., Takegawa, N., Kajino, M., Zhao, Y.,
25 Cubison, M. J., Jimenez, J. L., Vay, S., Diskin, G. S., Anderson, B., Wisthaler, A.,
26 Mikoviny, T., Fuelberg, H. E., Blake, D. R., Huey, G., Weinheimer, A. J., Knapp, D. J.
27 and Brune, W. H.: Emissions of black carbon, organic, and inorganic aerosols from
28 biomass burning in North America and Asia in 2008, *J. Geophys. Res. Atmospheres*,
29 116(D8), D08204, doi:10.1029/2010JD015152, 2011.

1 Korolev, A. and Isaac, G. A.: Relative Humidity in Liquid, Mixed-Phase, and Ice Clouds,
2 J. Atmospheric Sci., 63(11), 2865–2880, doi:10.1175/JAS3784.1, 2006.

3 Korolev, A. V., Isaac, G. A., Cober, S. G., Strapp, J. W. and Hallett, J.: Microphysical
4 characterization of mixed-phase clouds, Q. J. R. Meteorol. Soc., 129(587), 39–65,
5 doi:10.1256/qj.01.204, 2003.

6 Korolev, A. V., Emery, E. F., Strapp, J. W., Cober, S. G., Isaac, G. A., Wasey, M. and
7 Marcotte, D.: Small Ice Particles in Tropospheric Clouds: Fact or Artifact? Airborne
8 Icing Instrumentation Evaluation Experiment, Bull. Am. Meteorol. Soc., 92(8), 967–973,
9 doi:10.1175/2010BAMS3141.1, 2011.

10 Korolev, A. V., Strapp, J. W., Isaac, G. A. and Nevzorov, A. N.: The Nevzorov Airborne
11 Hot-Wire LWC–TWC Probe: Principle of Operation and Performance Characteristics, J.
12 Atmospheric Ocean. Technol., 15(6), 1495–1510, doi:10.1175/1520-
13 0426(1998)015<1495:TNAHWL>2.0.CO;2, 1998.

14 Kupiszewski, P., Leck, C., Tjernström, M., Sjogren, S., Sedlar, J., Graus, M., Müller, M.,
15 Brooks, B., Swietlicki, E., Norris, S. and Hansel, A.: Vertical profiling of aerosol
16 particles and trace gases over the central Arctic Ocean during summer, Atmos Chem
17 Phys, 13(24), 12405–12431, doi:10.5194/acp-13-12405-2013, 2013.

18 Kuwata, M., Kondo, Y., and Takegawa, N.: Critical condensed mass for activation of
19 black carbon as cloud condensation nuclei in Tokyo, J. Geophys. Res., 114, D20202,
20 doi:10.1029/2009JD012086, 2009.

21 Lance, S., Shupe, M. D., Feingold, G., Brock, C. A., Cozic, J., Holloway, J. S.,
22 Moore, R. H., Nenes, A., Schwarz, J. P., Spackman, J. R., Froyd, K. D., Murphy, D. M.,
23 Brioude, J., Cooper, O. R., Stohl, A., and Burkhardt, J. F.: Cloud condensation nuclei as a
24 modulator of ice processes in Arctic mixed-phase clouds, Atmos. Chem. Phys., 11, 8003-
25 8015, doi:10.5194/acp-11-8003-2011, 2011.

26 Latham, T. L., Beyersdorf, A. J., Thornhill, K. L., Winstead, E. L., Cubison, M. J.,
27 Hecobian, A., Jimenez, J. L., Weber, R. J., Anderson, B. E. and Nenes, A.: Analysis of
28 CCN activity of Arctic aerosol and Canadian biomass burning during summer 2008,
29 Atmos Chem Phys, 13(5), 2735–2756, doi:10.5194/acp-13-2735-2013, 2013.

1 Lawler, M. J., Whitehead, J., O'Dowd, C., Monahan, C., McFiggans, G. and Smith, J. N.:
2 Composition of 15–85 nm particles in marine air, *Atmos Chem Phys*, 14(21), 11557–
3 11569, doi:10.5194/acp-14-11557-2014, 2014.

4 Lawson, R. P., Baker, B. A., Schmitt, C. G. and Jensen, T. L.: An overview of
5 microphysical properties of Arctic clouds observed in May and July 1998 during FIRE
6 ACE, *J. Geophys. Res. Atmospheres*, 106(D14), 14989–15014,
7 doi:10.1029/2000JD900789, 2001.

8 Leaitch, W. R., Sharma, S., Huang, L., Toom-Sauntry, D., Chivulescu, A., Macdonald, A.
9 M., von Salzen, K., Pierce, J. R., Bertram, A. K., Schroder, J. C., Shantz, N. C., Chang,
10 R. Y.-W. and Norman, A.-L.: Dimethyl sulfide control of the clean summertime Arctic
11 aerosol and cloud, *Elem. Sci. Anthr.*, 1, 000017, doi:10.12952/journal.elementa.000017,
12 2013.

13 Lebsock, M. D., Stephens, G. L. and Kummerow, C.: Multisensor satellite observations
14 of aerosol effects on warm clouds, *J. Geophys. Res. Atmospheres*, 113(D15), D15205,
15 doi:10.1029/2008JD009876, 2008.

16 Leck, C. and Bigg, E. K.: Aerosol production over remote marine areas-A new route,
17 *Geophys. Res. Lett.*, 26(23), 3577–3580, doi:10.1029/1999GL010807, 1999.

18 Leck, C. and Bigg, E. K.: Biogenic particles in the surface microlayer and overlaying
19 atmosphere in the central Arctic Ocean during summer, *Tellus B*, 57(4), 305–316,
20 doi:10.1111/j.1600-0889.2005.00148.x, 2005.

21 Lihavainen, H., Kerminen, V.-M. and Remer, L. A.: Aerosol-cloud interaction
22 determined by both in situ and satellite data over a northern high-latitude site, *Atmos*
23 *Chem Phys*, 10(22), 10987–10995, doi:10.5194/acp-10-10987-2010, 2010.

24 Lindsey, D. T. and Fromm, M.: Evidence of the cloud lifetime effect from wildfire-
25 induced thunderstorms, *Geophys. Res. Lett.*, 35(22), L22809,
26 doi:10.1029/2008GL035680, 2008.

27 Lohmann, U. and Leck, C.: Importance of submicron surface-active organic aerosols for
28 pristine Arctic clouds, *Tellus B*, 57(3), doi:10.3402/tellusb.v57i3.16534, 2005.

1 Lubin, D. and Vogelmann, A. M.: A climatologically significant aerosol longwave
2 indirect effect in the Arctic, *Nature*, 439(7075), 453–456, doi:10.1038/nature04449,
3 2006.

4 Matsui, H., Kondo, Y., Moteki, N., Takegawa, N., Sahu, L. K., Zhao, Y., Fuelberg, H. E.,
5 Sessions, W. R., Diskin, G., Blake, D. R., Wisthaler, A. and Koike, M.: Seasonal
6 variation of the transport of black carbon aerosol from the Asian continent to the Arctic
7 during the ARCTAS aircraft campaign, *J. Geophys. Res. Atmospheres*, 116(D5),
8 doi:10.1029/2010JD015067, 2011.

9 McComiskey, A. and Feingold, G.: Quantifying error in the radiative forcing of the first
10 aerosol indirect effect, *Geophys. Res. Lett.*, 35(2), L02810, doi:10.1029/2007GL032667,
11 2008.

12 McComiskey, A. and Feingold, G.: The scale problem in quantifying aerosol indirect
13 effects, *Atmos Chem Phys*, 12(2), 1031–1049, doi:10.5194/acp-12-1031-2012, 2012.

14 McComiskey, A., Feingold, G., Frisch, A. S., Turner, D. D., Miller, M. A., Chiu, J. C.,
15 Min, Q. and Ogren, J. A.: An assessment of aerosol-cloud interactions in marine stratus
16 clouds based on surface remote sensing, *J. Geophys. Res. Atmospheres*, 114(D9),
17 D09203, doi:10.1029/2008JD011006, 2009.

18 McConnell, J. R., Edwards, R., Kok, G. L., Flanner, M. G., Zender, C. S., Saltzman, E.,
19 S., Banta, J. R., Pasteris, D. R., Carter, M. M. and Kahl, J. D. W.: 20th-Century Industrial
20 Black Carbon Emissions Altered Arctic Climate Forcing, *Science*, 317(5843), 1381–
21 1384, doi:10.1126/science.1144856, 2007.

22 McFarquhar, G. M., Ghan, S., Verlinde, J., Korolev, A., Strapp, J. W., Schmid, B.,
23 Tomlinson, J. M., Wolde, M., Brooks, S. D., Cziczo, D., Dubey, M. K., Fan, J., Flynn, C.,
24 Gultepe, I., Hubbe, J., Gilles, M. K., Laskin, A., Lawson, P., Leaitch, W. R., Liu, P., Liu,
25 X., Lubin, D., Mazzoleni, C., Macdonald, A.-M., Moffet, R. C., Morrison, H.,
26 Ovchinnikov, M., Shupe, M. D., Turner, D. D., Xie, S., Zelenyuk, A., Bae, K., Freer, M.
27 and Glen, A.: Indirect and semi-direct aerosol campaign: The Impact of Arctic Aerosols
28 on Clouds, *Bull. Am. Meteorol. Soc.*, 92(2), 183–+, 2011.

1 McFarquhar, G. M., Zhang, G., Poellot, M. R., Kok, G. L., McCoy, R., Tooman, T.,
2 Fridlind, A. and Heymsfield, A. J.: Ice properties of single-layer stratocumulus during the
3 Mixed-Phase Arctic Cloud Experiment: 1. Observations, *J. Geophys. Res. Atmospheres*,
4 112(D24), D24201, doi:10.1029/2007JD008633, 2007.

5 McNaughton, C. S., Clarke, A. D., Freitag, S., Kapustin, V. N., Kondo, Y., Moteki, N.,
6 Sahu, L., Takegawa, N., Schwarz, J. P., Spackman, J. R., Watts, L., Diskin, G., Podolske,
7 J., Holloway, J. S., Wisthaler, A., Mikoviny, T., de Gouw, J., Warneke, C., Jimenez, J.,
8 Cubison, M., Howell, S. G., Middlebrook, A., Bahreini, R., Anderson, B. E., Winstead,
9 E., Thornhill, K. L., Lack, D., Cozic, J. and Brock, C. A.: Absorbing aerosol in the
10 troposphere of the Western Arctic during the 2008 ARCTAS/ARCPAC airborne field
11 campaigns, *Atmos Chem Phys*, 11(15), 7561–7582, doi:10.5194/acp-11-7561-2011,
12 2011.

13 Moore, R. H., Bahreini, R., Brock, C. A., Froyd, K. D., Cozic, J., Holloway, J. S.,
14 Middlebrook, A. M., Murphy, D. M. and Nenes, A.: Hygroscopicity and composition of
15 Alaskan Arctic CCN during April 2008, *Atmos Chem Phys*, 11(22), 11807–11825,
16 doi:10.5194/acp-11-11807-2011, 2011.

17 Moore, R. H., Karydis, V. A., Capps, S. L., Lathem, T. L. and Nenes, A.: Droplet number
18 uncertainties associated with CCN: an assessment using observations and a global model
19 adjoint, *Atmos Chem Phys*, 13(8), 4235–4251, doi:10.5194/acp-13-4235-2013, 2013.

20 Morales, R. and Nenes, A.: Characteristic updrafts for computing distribution-averaged
21 cloud droplet number and stratocumulus cloud properties, *J. Geophys. Res. Atmospheres*,
22 115(D18), D18220, doi:10.1029/2009JD013233, 2010.

23 Morales, R., Nenes, A., Jonsson, H., Flagan, R. C. and Seinfeld, J. H.: Evaluation of an
24 entraining droplet activation parameterization using in situ cloud data, *J. Geophys. Res.*
25 *Atmospheres*, 116(D15), D15205, doi:10.1029/2010JD015324, 2011.

26 Moritz, M. A., Parisien, M.-A., Batllori, E., Krawchuk, M. A., Van Dorn, J., Ganz, D. J.
27 and Hayhoe, K.: Climate change and disruptions to global fire activity, *Ecosphere*, 3(6),
28 art49, doi:10.1890/ES11-00345.1, 2012.

1 Morrison, H., de Boer, G., Feingold, G., Harrington, J., Shupe, M. D. and Sulia, K.:
2 Resilience of persistent Arctic mixed-phase clouds, *Nat. Geosci.*, 5(1), 11–17,
3 doi:10.1038/ngeo1332, 2012.

4 O’Dowd, C., Monahan, C. and Dall’Osto, M.: On the occurrence of open ocean particle
5 production and growth events, *Geophys. Res. Lett.*, 37(19), L19805,
6 doi:10.1029/2010GL044679, 2010.

7 Orellana, M. V., Matrai, P. A., Leck, C., Rauschenberg, C. D., Lee, A. M. and Coz, E.:
8 Marine microgels as a source of cloud condensation nuclei in the high Arctic, *Proc. Natl.*
9 *Acad. Sci.*, 108(33), 13612–13617, doi:10.1073/pnas.1102457108, 2011.

10 Oshima, N., M. Koike, Y. Zhang, and Y. Kondo: Aging of black carbon in outflow from
11 anthropogenic sources using a mixing state resolved model: 2. Aerosol optical properties
12 and cloud condensation nuclei activities, *J. Geophys. Res.*, 114, D18202,
13 doi:10.1029/2008JD011681, 2009.

14 Peng, Y., Lohmann, U., Leaitch, R., Banic, C. and Couture, M.: The cloud albedo-cloud
15 droplet effective radius relationship for clean and polluted clouds from RACE and
16 FIRE.ACE, *J. Geophys. Res. Atmospheres*, 107(D11), AAC 1–1,
17 doi:10.1029/2000JD000281, 2002.

18 Platnick, S., King, M. D., Ackerman, S. A., Menzel, W. P., Baum, B. A., Riedi, J. C. and
19 Frey, R. A.: The MODIS cloud products: algorithms and examples from Terra, *IEEE*
20 *Trans. Geosci. Remote Sens.*, 41(2), 459 – 473, doi:10.1109/TGRS.2002.808301, 2003.

21 Quinn, P. K., Bates, T. S., Miller, T. L., Coffman, D. J., Johnson, J. E., Harris, J. M.,
22 Ogren, J. A., Forbes, G., Anderson, T. L., Covert, D. S. and Rood, M. J.: Surface
23 submicron aerosol chemical composition: What fraction is not sulfate?, *J. Geophys. Res.*
24 *Atmospheres*, 105(D5), 6785–6805, doi:10.1029/1999JD901034, 2000.

25 Quinn, P. K., Miller, T. L., Bates, T. S., Ogren, J. A., Andrews, E. and Shaw, G. E.: A 3-
26 year record of simultaneously measured aerosol chemical and optical properties at
27 Barrow, Alaska, *J. Geophys. Res.*, 107(D11), 4130, doi:10.1029/2001JD001248, 2002.

28 R Core Team.: R: A language and environment for statistical computing. R Foundation
29 for Statistical Computing, Vienna, Austria. URL <http://www.R-project.org/>, 2013.

1 Raatikainen, T., Moore, R. H., Latham, T. L. and Nenes, A.: A coupled observation –
2 modeling approach for studying activation kinetics from measurements of CCN activity,
3 *Atmos Chem Phys*, 12(9), 4227–4243, doi:10.5194/acp-12-4227-2012, 2012.

4 Rangno, A. L. and Hobbs, P. V.: Ice particles in stratiform clouds in the Arctic and
5 possible mechanisms for the production of high ice concentrations, *J. Geophys. Res.*
6 *Atmospheres*, 106(D14), 15065–15075, doi:10.1029/2000JD900286, 2001.

7 Riemer, N., Vogel, H., and Vogel, B.: Soot aging time scales in polluted regions during
8 day and night, *Atmos. Chem. Phys.*, 4, 1885-1893, doi:10.5194/acp-4-1885-2004, 2004.

9 Rosenfeld, D., Fromm, M., Trentmann, J., Luderer, G., Andreae, M. O. and Servranckx,
10 R.: The Chisholm firestorm: observed microstructure, precipitation and lightning activity
11 of a pyro-cumulonimbus, *Atmos Chem Phys*, 7(3), 645–659, doi:10.5194/acp-7-645-
12 2007, 2007.

13 Rosenfeld, D., Wang, H. and Rasch, P. J.: The roles of cloud drop effective radius and
14 LWP in determining rain properties in marine stratocumulus, *Geophys. Res. Lett.*,
15 39(13), L13801, doi:10.1029/2012GL052028, 2012.

16 Rosenfeld, D., Fischman, B., Zheng, Y., Goren, T. and Giguzin, D.: Combined satellite
17 and radar retrievals of drop concentration and CCN at convective cloud base, *Geophys.*
18 *Res. Lett.*, 41(9), 2014GL059453, doi:10.1002/2014GL059453, 2014.

19 Sakamoto, K. M., Allan, J. D., Coe, H., Taylor, J. W., Duck, T. J. and Pierce, J. R.: Aged
20 boreal biomass-burning aerosol size distributions from BORTAS 2011, *Atmos Chem*
21 *Phys*, 15(4), 1633–1646, doi:10.5194/acp-15-1633-2015, 2015.

22 Sachse, G. W., Hill, G. F., Wade, L. O., and Perry, M. G.: Fast re- sponse, high precision
23 carbon monoxide sensor using a tunable diode laser absorption technique, *J. Geophys.*
24 *Res.*, 92, 2071– 2081, 1987.

25 Seinfeld, J. H. and Pandis, S. N.: *Atmospheric Chemistry and Physics: From Air*
26 *Pollution to Climate Change*, John Wiley and Sons, New York., 1998.

27 Sen, P. K.: Estimates of the Regression Coefficient Based on Kendall’s Tau, *J. Am. Stat.*
28 *Assoc.*, 63(324), 1379–1389, doi:10.1080/01621459.1968.10480934, 1968.

1 Shantz, N. C., Gultepe, I., Andrews, E., Zelenyuk, A., Earle, M. E., Macdonald, A. M.,
2 Liu, P. S. K. and Leitch, W. R.: Optical, physical, and chemical properties of springtime
3 aerosol over Barrow Alaska in 2008, *Int. J. Climatol.*, 34(10), 3125–3138,
4 doi:10.1002/joc.3898, 2014.

5 Shantz, N. C., Gultepe, I., Liu, P. S. K., Earle, M. E. and Zelenyuk, A.: Spatial and
6 temporal variability of aerosol particles in Arctic spring, *Q. J. R. Meteorol. Soc.*,
7 138(669), 2229–2240, doi:10.1002/qj.1940, 2012.

8 Shao, H. and Liu, G.: Influence of mixing on evaluation of the aerosol first indirect
9 effect, *Geophys. Res. Lett.*, 33(14), L14809, doi:10.1029/2006GL026021, 2006.

10 Shaw, G. E.: The Arctic Haze Phenomenon, *Bull. Am. Meteorol. Soc.*, 76(12), 2403–
11 2413, doi:10.1175/1520-0477(1995)076<2403:TAHP>2.0.CO;2, 1995.

12 Shinozuka, Y. and Redemann, J.: Horizontal variability of aerosol optical depth observed
13 during the ARCTAS airborne experiment, *Atmos Chem Phys*, 11(16), 8489–8495,
14 doi:10.5194/acp-11-8489-2011, 2011.

15 Singh, H. B., Anderson, B. E., Brune, W. H., Cai, C., Cohen, R. C., Crawford, J. H.,
16 Cubison, M. J., Czech, E. P., Emmons, L., Fuelberg, H. E., Huey, G., Jacob, D. J.,
17 Jimenez, J. L., Kaduwela, A., Kondo, Y., Mao, J., Olson, J. R., Sachse, G. W., Vay, S.
18 A., Weinheimer, A., Wennberg, P. O. and Wisthaler, A.: Pollution influences on
19 atmospheric composition and chemistry at high northern latitudes: Boreal and California
20 forest fire emissions, *Atmos. Environ.*, 44(36), 4553–4564,
21 doi:10.1016/j.atmosenv.2010.08.026, 2010.

22 Soja, A. J., Stocks, B., Maczek, P., Fromm, M., Servranckx, R. and Turetsky, M.:
23 ARCTAS: the perfect smoke., *Can. Smoke Newsl.*, 2–7, 2008.

24 Stephens, G. L.: Radiation Profiles in Extended Water Clouds. I: Theory, *J. Atmospheric*
25 *Sci.*, 35(11), 2111–2122, doi:10.1175/1520-0469(1978)035<2111:RPIEWC>2.0.CO;2,
26 1978.

27 Stocks, B. J., Fosberg, M. A., Lynham, T. J., Mearns, L., Wotton, B. M., Yang, Q., Jin,
28 J.-Z., Lawrence, K., Hartley, G. R., Mason, J. A. and McKENNEY, D. W.: Climate

1 Change and Forest Fire Potential in Russian and Canadian Boreal Forests, *Clim. Change*,
2 38(1), 1–13, doi:10.1023/A:1005306001055, 1998.

3 Stohl, A., Andrews, E., Burkhardt, J. F., Forster, C., Herber, A., Hoch, S. W., Kowal, D.,
4 Lunder, C., Mefford, T., Ogren, J. A., Sharma, S., Spichtinger, N., Stebel, K., Stone, R.,
5 Ström, J., Tørseth, K., Wehrli, C. and Yttri, K. E.: Pan-Arctic enhancements of light
6 absorbing aerosol concentrations due to North American boreal forest fires during
7 summer 2004, *J. Geophys. Res.*, 111(D22), D22214, doi:10.1029/2006JD007216, 2006.

8 Stohl, A., Berg, T., Burkhardt, J. F., Fjårraa, A. M., Forster, C., Herber, A., Hov, Ø.,
9 Lunder, C., McMillan, W. W., Oltmans, S., Shiobara, M., Simpson, D., Solberg, S.,
10 Stebel, K., Ström, J., Tørseth, K., Treffeisen, R., Virkkunen, K. and Yttri, K. E.: Arctic
11 smoke – record high air pollution levels in the European Arctic due to agricultural fires in
12 Eastern Europe in spring 2006, *Atmos Chem Phys*, 7(2), 511–534, doi:10.5194/acp-7-
13 511-2007, 2007.

14 Stone, R. S.: Variations in western Arctic temperatures in response to cloud radiative and
15 synoptic-scale influences, *J. Geophys. Res. Atmospheres*, 102(D18), 21769–21776,
16 doi:10.1029/97JD01840, 1997.

17 Strapp, J. W., Leaitch, W. R. and Liu, P. S. K.: Hydrated and Dried Aerosol-Size-
18 Distribution Measurements from the Particle Measuring Systems FSSP-300 Probe and
19 the Deiced PCASP-100X Probe, *J. Atmospheric Ocean. Technol.*, 9(5), 548–555,
20 doi:10.1175/1520-0426(1992)009<0548:HADASD>2.0.CO;2, 1992.

21 Ström, J., Engvall, A.-C., Delbart, F., Krejci, R. and Treffeisen, R.: On small particles in
22 the Arctic summer boundary layer: observations at two different heights near Ny-
23 Ålesund, Svalbard, *Tellus B*, 61(2), doi:10.3402/tellusb.v61i2.16845, 2009.

24 Tao, W.-K., Chen, J.-P., Li, Z., Wang, C. and Zhang, C.: Impact of aerosols on
25 convective clouds and precipitation, *Rev. Geophys.*, 50(2), RG2001,
26 doi:10.1029/2011RG000369, 2012.

27 Theil, H.: A rank-invariant method of linear and polynomial regression analysis, *Proc R*
28 *Neth Acad Sci LIII*, 1397–1412, 1950.

1 Tietze, K., Riedi, J., Stohl, A. and Garret, T. J.: Space-based evaluation of interactions
2 between aerosols and low-level Arctic clouds during the Spring and Summer of 2008,
3 *Atmospheric Chem. Phys.*, 11, 3359–3373, doi:10.5194/acp-11-3359-2011, 2011.

4 Tunved, P., Ström, J. and Krejci, R.: Arctic aerosol life cycle: linking aerosol size
5 distributions observed between 2000 and 2010 with air mass transport and precipitation at
6 Zeppelin station, Ny-Ålesund, Svalbard, *Atmos Chem Phys*, 13(7), 3643–3660,
7 doi:10.5194/acp-13-3643-2013, 2013.

8 Twomey, S.: The Influence of Pollution on the Shortwave Albedo of Clouds, *J.*
9 *Atmospheric Sci.*, 34(7), 1149–1152, doi:10.1175/1520-
10 0469(1977)034<1149:TIOPOT>2.0.CO;2, 1977.

11 Vavrus, S., Holland, M. M. and Bailey, D. A.: Changes in Arctic clouds during intervals
12 of rapid sea ice loss, *Clim. Dyn.*, 36(7-8), 1475–1489, doi:10.1007/s00382-010-0816-0,
13 2010.

14 Warneke, C., Bahreini, R., Brioude, J., Brock, C. A., Gouw, J. A. de, Fahey, D. W.,
15 Froyd, K. D., Holloway, J. S., Middlebrook, A., Miller, L., Montzka, S., Murphy, D. M.,
16 Peischl, J., Ryerson, T. B., Schwarz, J. P., Spackman, J. R. and Veres, P.: Biomass
17 burning in Siberia and Kazakhstan as an important source for haze over the Alaskan
18 Arctic in April 2008, *Geophys. Res. Lett.*, 36(2), L02813, doi:10.1029/2008GL036194,
19 2009.

20 Warneke, C., Froyd, K. D., Brioude, J., Bahreini, R., Brock, C. A., Cozic, J., de Gouw, J.
21 A., Fahey, D. W., Ferrare, R., Holloway, J. S., Middlebrook, A. M., Miller, L., Montzka,
22 S., Schwarz, J. P., Sodemann, H., Spackman, J. R. and Stohl, A.: An important
23 contribution to springtime Arctic aerosol from biomass burning in Russia, *Geophys. Res.*
24 *Lett.*, 37, 2010.

25 Wisthaler, A., Hansel, A., Dickerson, R. R. and Crutzen, P. J.: Organic trace gas
26 measurements by PTR-MS during INDOEX 1999, *J. Geophys. Res. Atmospheres*,
27 107(D19), 8024, doi:10.1029/2001JD000576, 2002.

28 Zelenyuk, A., Yang, J., Choi, E. and Imre, D.: SPLAT II: An Aircraft Compatible, Ultra-
29 Sensitive, High Precision Instrument for In-Situ Characterization of the Size and

1 Composition of Fine and Ultrafine Particles, *Aerosol Sci. Technol.*, 43(5), 411–424,
2 doi:10.1080/02786820802709243, 2009.

3 Zelenyuk, A., Imre, D., Earle, M., Easter, R., Korolev, A., Leaitch, R., Liu, P.,
4 Macdonald, A. M., Ovchinnikov, M. and Strapp, W.: In Situ Characterization of Cloud
5 Condensation Nuclei, Interstitial, and Background Particles Using the Single Particle
6 Mass Spectrometer, SPLAT II†, *Anal. Chem.*, 82(19), 7943–7951,
7 doi:10.1021/ac1013892, 2010.

8 Zelenyuk, A., Imre, D., Wilson, J., Zhang, Z., Wang, J. and Mueller, K.: Airborne single
9 particle mass spectrometers (SPLAT II & miniSPLAT) and new software for data
10 visualization and analysis in a geo-spatial context, *J. Am. Soc. Mass Spectrom.*, 26(2),
11 257–270, doi:10.1007/s13361-014-1043-4, 2015.

12 Zhao, C. and Garrett, T. J.: Effects of Arctic haze on surface cloud radiative forcing,
13 *Geophys. Res. Lett.*, 2014GL062015, doi:10.1002/2014GL062015, 2015.

14 Zhao, C., Klein, S. A., Xie, S., Liu, X., Boyle, J. S. and Zhang, Y.: Aerosol first indirect
15 effects on non-precipitating low-level liquid cloud properties as simulated by CAM5 at
16 ARM sites, *Geophys. Res. Lett.*, 39(8), L08806, doi:10.1029/2012GL051213, 2012.

17 Zhou, J., Swietlicki, E., Berg, O. H., Aalto, P. P., Hämeri, K., Nilsson, E. D. and Leck,
18 C.: Hygroscopic properties of aerosol particles over the central Arctic Ocean during
19 summer, *J. Geophys. Res. Atmospheres*, 106(D23), 32111–32123,
20 doi:10.1029/2000JD900426, 2001.

21 Zuidema, P., Baker, B., Han, Y., Intrieri, J., Key, J., Lawson, P., Matrosov, S., Shupe,
22 M., Stone, R. and Uttal, T.: An Arctic Springtime Mixed-Phase Cloudy Boundary Layer
23 Observed during SHEBA, *J. Atmospheric Sci.*, 62(1), 160–176, doi:10.1175/JAS-3368.1,
24 2005.

25

1 Table 1. Instrumentation used in this study from the ARCTAS dataset. Data were
 2 collected at 1-second resolution, unless noted otherwise.

ARCTAS-A 1-19 April; -CARB 29 June; -B 1-13 July, 2008			
	Instrument	Range	Uncertainty
N_{liq}, r_e, and LWC	Cloud, Aerosol and Precipitation Spectrometer - Cloud and Aerosol Spectrometer (CAPS-CAS)	0.5-50 μm	20% ^a
phase	none (see text)	liquid only	n.a.
CN	TSI Condensation Particle Counter (CPC) 3010	> 0.01 μm	precision 5%
	TSI CPC 3025	> 0.003 μm	precision 10%
	TSI Aerodynamic Particle Sizer (APS) 3321	0.583-7.75 μm	n.a.
	DMT Ultra High Sensitivity Aerosol Spectrometer (UHSAS)	0.0609-0.986 μm	~5%, but increases in air with > 3000 particles cm ⁻³ (Cai et al., 2008)
Temperature	Rosemount 102 E4AL	-65 to +35 °C	±1°C
Relative humidity	Aircraft-Integrated Meteorological Measurement System (AIMMS-20)	--	2%
CCN	DMT continuous-flow, streamwise thermal-gradient CCN counter	--	7–16 % (Moore et al., 2011)
CO	Tunable Diode Laser Absorption Spectrometer (TDLAS)	--	±2% (Sachse et al., 1987)
Submicron sulfate^b	Time-of-Flight Aerosol Mass Spectrometer	--	±35% (DeCarlo et al. (2008))
Submicron OA^b	Time-of-Flight Aerosol Mass Spectrometer	--	38% (Huffman et al. (2005))
BC mass^b	Single-Particle Soot Photometer (SP2)	--	±10% (Moteki and Kondo, 2008)
CH₃CN	Proton Transfer Reaction – Mass Spectrometer (PTR-MS)	--	±10% (Wisthaler et al., 2002)
CH₂Cl₂^c	Electron Capture Detection and Mass Spectrometer	--	+/-10% or +/-2 pptv (Colman et al., 2001)
Total backscatter (550 nm)^b	TSI 3563 Integrating Nephelometer	> 0.1 Mm ⁻¹	0.5 Mm ⁻¹
Submicron scatter (550 nm)^b	Radiance Research Model M903 Nephelometer	1 Mm ⁻¹	0.5 Mm ⁻¹

3 ^aBased on pre- and post-campaign comparisons with sized glass and latex spheres

4 ^bData were collected at 10 s resolution

5 ^cData were collected at ~40 s resolution

6

- 1 Table 2. Instrumentation used in this study from the ISDAC dataset. Data were collected
 2 at 1-second resolution.

ISDAC, 1-29 April, 2008			
	Instrument	Range	Uncertainty
N_{liq}, r_e, LWC	DMT Cloud Droplet Probe (CDP)	2-50 μm	~20% (Earle et al., 2011)
^aN_{liq}, LWC, r_e	Forward Scattering Spectrometer Probe (FSSP) model 100	0.3-47 μm	~17% (N _{liq}), ~34% (LWC, r _e) (Baumgardner, 1983)
phase	Cloud Particle Imager (CPI)	40 μm - 2 mm	n.a.
CN	PMS airborne Passive Cavity Aerosol Spectrometer Probe (PCASP)-100X	~ 0.12-3 μm	7% (Earle et al., 2011)
	TSI CPC 3775	> 0.004 μm	±10% (Shantz et al., 2014)
Temperature	Rosemont 102 probe	-65 to +35 °C	±1°C
CCN	DMT continuous-flow, streamwise thermal-gradient CCN counter (reported between 14-37% supersaturation)	--	7-16 % (Moore et al., 2011)
Total and submicron dry backscatter (550 nm)	TSI 3563 Integrating Nephelometer	> 0.1 M m ⁻¹	1-2±0.5 M m ⁻¹

- 3 ^aFor days when high quality CDP data were unavailable, following Earle et al. (2011)

1 Table 3. Instrumentation used in this study from the NRC FIRE.ACE dataset. Data were
 2 collected at 1-second resolution.

3

NRC FIRE.ACE, 1-29 April, 1998			
	Instrument	Range	Uncertainty
N_{liq}	FSSP-100	0.3-47 μm	$\sim 17\%$ (Baumgardner, 1983)
LWC, r_e	FSSP-100	0.3-47	up to 25% (Peng et al., 2002)
LWC	King probe	0.05-3 g m^{-3}	$\pm 10\%$ or larger (Peng et al., 2002)
	Nevzorov probe	$\sim 0.006\text{-}1 \text{ g m}^{-3}$	$\pm 15\%$ (Korolev et al., 1998)
phase	CPI	40 μm - 2 mm	not available
Temperature	Rosemont probe	-65 to $+35$ $^{\circ}\text{C}$	$\pm 1^{\circ}\text{C}$ in-cloud, $\pm 2\text{-}3^{\circ}\text{C}$ out-of-cloud
CN	PCASP 100X	0.12-3 μm	7% (Earle et al., 2011)
CCN	Cloud condensation nucleus counter (reported at 57-72% supersaturation)	n.a.	$\pm 10\%$

4

5

1 Table 4. Instrumentation used in this study from the UW FIRE.ACE dataset. Data were
 2 collected at 1-second resolution.

3

UW FIRE.ACE, 19 May - 24 June, 1998			
	Instrument	Range	Uncertainty
N_{liq}	FSSP-100	0.3-47 μm	~17% (Baumgardner, 1983)
LWC, r_e	FSSP-100	0.3-47 μm	see Table 5
LWC	Gerber Scientific PVM-100X	0.01-0.75 g m^{-3}	12% (Garrett and Hobbs, 1999)
phase	CPI	40 μm - 2 mm	not available
CN	PCASP 100X	0.12-3 μm	7% (Earle et al., 2011)
Total dry backscatter (550 nm)	MS Electron Integrating Nephelometer	> 0.1 M m^{-1}	not available

4

1 Table 5. Comparison of LWC measurements (g m^{-3}) from various instruments.

2

Campaign	LWC determination method	<i>slope</i>	<i>y-intercept</i>	<i>R² value</i>
UW FIRE.ACE	FSSP vs. Gerber Scientific PVM-100X ^a (Gerber et al., 1994)	0.92	-0.018	0.88
NRC FIRE.ACE ^b	FSSP-124 vs. King probe (King et al., 1978)	1.08	-0.006	0.96
	FSSP-124 vs. Nevzorov probe (Korolev et al., 1998)	1.01	0.045	0.82
	Nevzorov vs. King	0.87	0.001	0.82

3

4 ^aFor Gerber LWC $< 0.5 \text{ g m}^{-3}$. Above that, the FSSP missed known rain/drizzle events
5 with larger droplets, and that began to impact the linear relationship.

6 ^bSamples with LWC $<$ the detection limit were not included.

7

1 Table 6. A comparison of background concentrations of biomass burning and pollution
 2 tracers as previously reported to those in the ARCTAS-B dataset in air masses that would
 3 be defined as background using only the CN_{PCASP} equivalent^a cutoff of ≤ 127 particles
 4 cm^{-3} . Data are out-of-cloud and from altitudes < 2.1 km due to instrument limitations
 5 above this level.

Tracer (units)	Median (interquartile range)	95th percentile	Previously reported background^b concentrations
CO (ppbv)	96 (96-109)	135	120-170 ^{f,i}
CH ₃ CN (ppbv)	0.08 (0.06-0.10)	0.19	0.1 ^{h,j}
BC ($\mu g C m^{-3}$)	0.001 (0.001-0.004)	0.016	0.029 ^f
Submicron SO ₄ ²⁻ ($\mu g m^{-3}$) ^c	0.010 (0.005-0.070)	0.33	0.1-0.9 ^{f,j,l}

6 ^a CN_{PCASP} values were not available in ARCTAS, and were thus approximated from the
 7 CN concentrations from the APS and UHSAS for the same size range as would be
 8 measured in the PCASP.

9 ^bSubmicron SO₄²⁻ concentrations are reflective of average, not background, conditions.

10 ^cFollowing Fisher et al., 2011, we assume ARCTAS submicron sea-salt SO₄²⁻ is
 11 negligible, and that total submicron SO₄²⁻ is approximately equal to submicron non
 12 seasalt-SO₄²⁻.

13 ^dStohl et al. (2007)

14 ^{e,f}Warneke et al. (2009, 2010)

15 ^gBrock et al. (2011)

16 ^hMoore et al. (2011)

17 ⁱShinozuka et al. (2015)

18 ^jLatham et al. (2013)

19 ^{k,l}Quinn et al. (2000, 2002)

20

- 1 Table 7. Median properties and ranges for all background and biomass burning cloud
 2 cases in the multi-campaign assessment.

Property	Background (n=19)	Biomass burning (n=8)
Aerosol number concentration (CN _{PCASP} ^a), cm ⁻³	42 (1-97)	584 (58-2001)
CCN, cm ⁻³	31 (6-332)	437 (68-6670)
Backscatter at 550 nm, Mm ⁻¹	0.7 (-0.19-1.13)	8.8 (0.3-44.1)
Temperature, °C	-5 (-20-7)	2 (-9-10)
Pressure, mbar	848 (505-995)	776 (687-909)
Liquid water content (LWC), g m ⁻³	0.07 (0.01-0.25)	0.03 (0.01-0.27)
Cloud droplet effective radius (r _e), μm	8.7 (5.7-12.6)	5.0 (1.9-7.8)
Droplet number concentration (N _{liq}), cm ⁻³	41 (12-525)	338 (188-782)

- 3
 4 ^aCN_{PCASP} equivalent data
 5

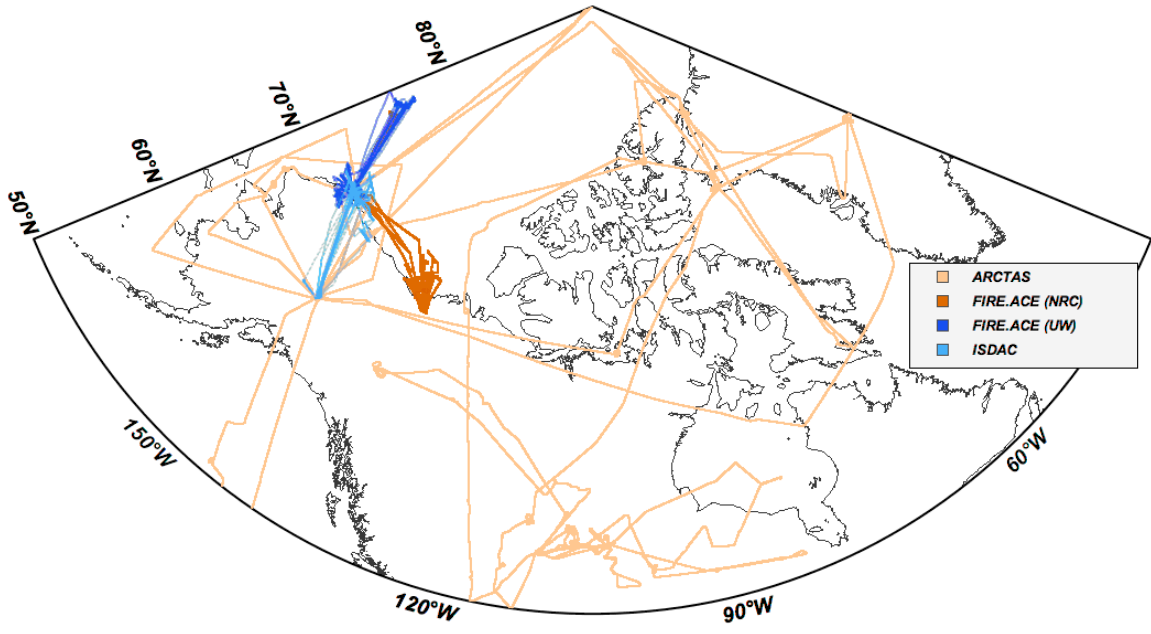
1 Table 8. Mean properties and ranges for the 1 July 2008 ARCTAS case study, including
 2 background, intermediate, and biomass burning cloud cases.

3

Property	Background (n=2)	Intermediate (n=3)	Biomass burning (n=2)
Aerosol number concentration (CN_{PCASP}^a), cm^{-3}	249 (107-390)	294 (147-427)	2604 (2207-3001)
CCN, cm^{-3}	545 (205-592)	722 (462-908)	10879 (10348-11411)
Backscatter at 550 nm, Mm^{-1}	1.7 (0.9-2.5)	3.3 (1.6-4.7)	35.7 (31.2-40.2)
Temperature, $^{\circ}C$	0.8 (0.2-0.9)	0.1 (-0.1-3.1)	2.8 (2.4-3.1)
Pressure, mbar	766 (762-770)	786 (763-826)	808
Liquid water content (LWC), $g\ m^{-3}$	0.07 (0.03-0.12)	0.02 (0.01-0.04)	0.01 (0.01-0.02)
Cloud droplet effective radius (r_e), μm	4.8 (3.7-5.8)	2.6 (2.1-3.3)	1.9 (1.9-2.0)
Droplet number concentration (N_{liq}), cm^{-3}	454 (384-525)	749 (621-907)	936 (824-1048)

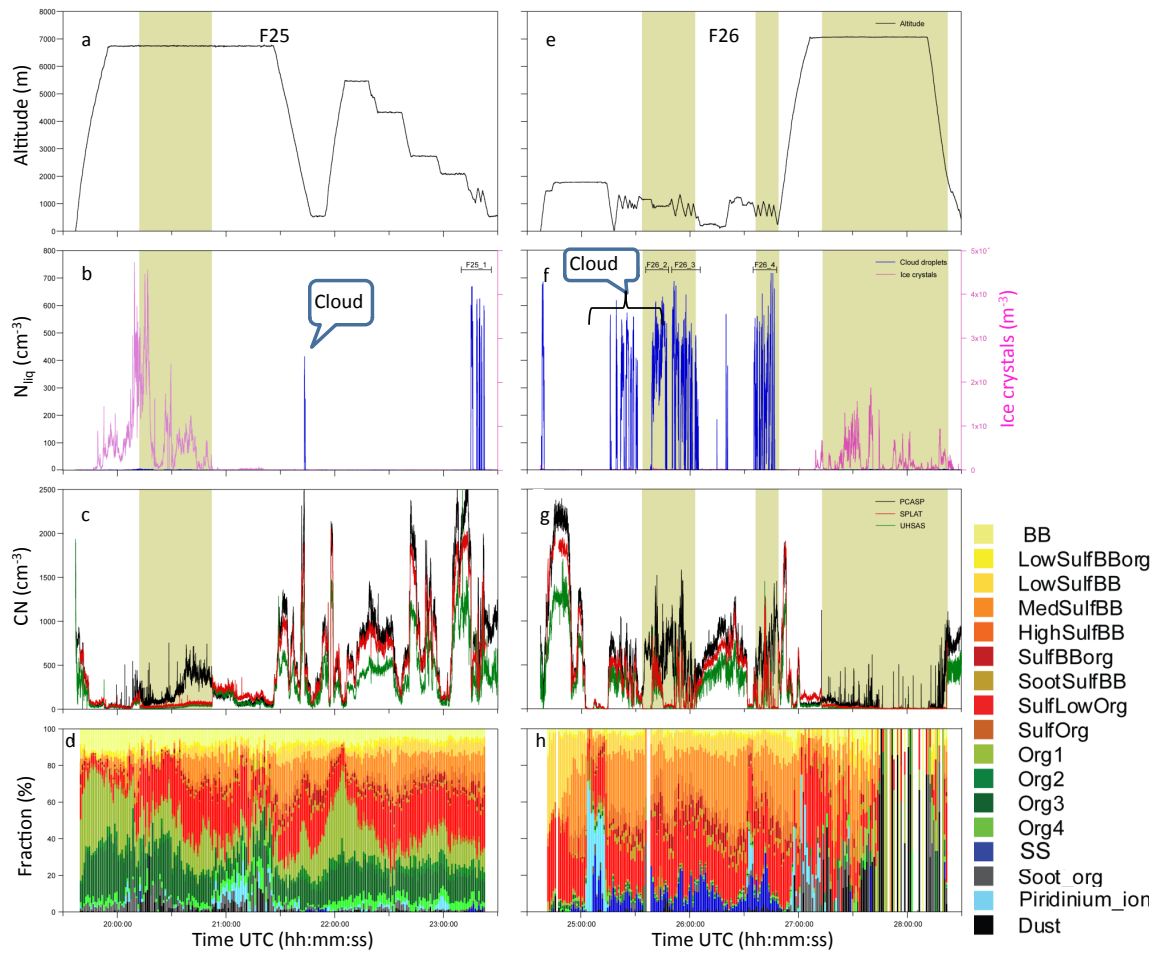
4

5 ^aOr CN_{PCASP} equivalent for ARCTAS data



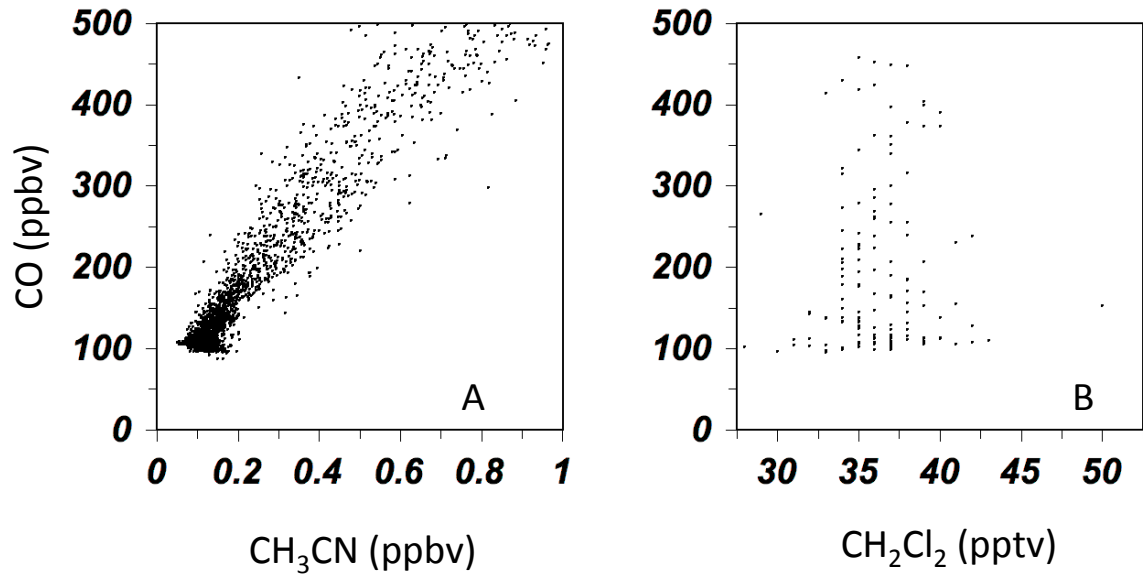
1
2

3 Figure 1. Sampling locations for the following campaigns: ARCTAS (light orange), NRC
4 FIRE.ACE (dark orange), UW FIRE.ACE (dark blue), and ISDAC (light blue). The
5 locations of clouds sampled are shown in Fig. 4.



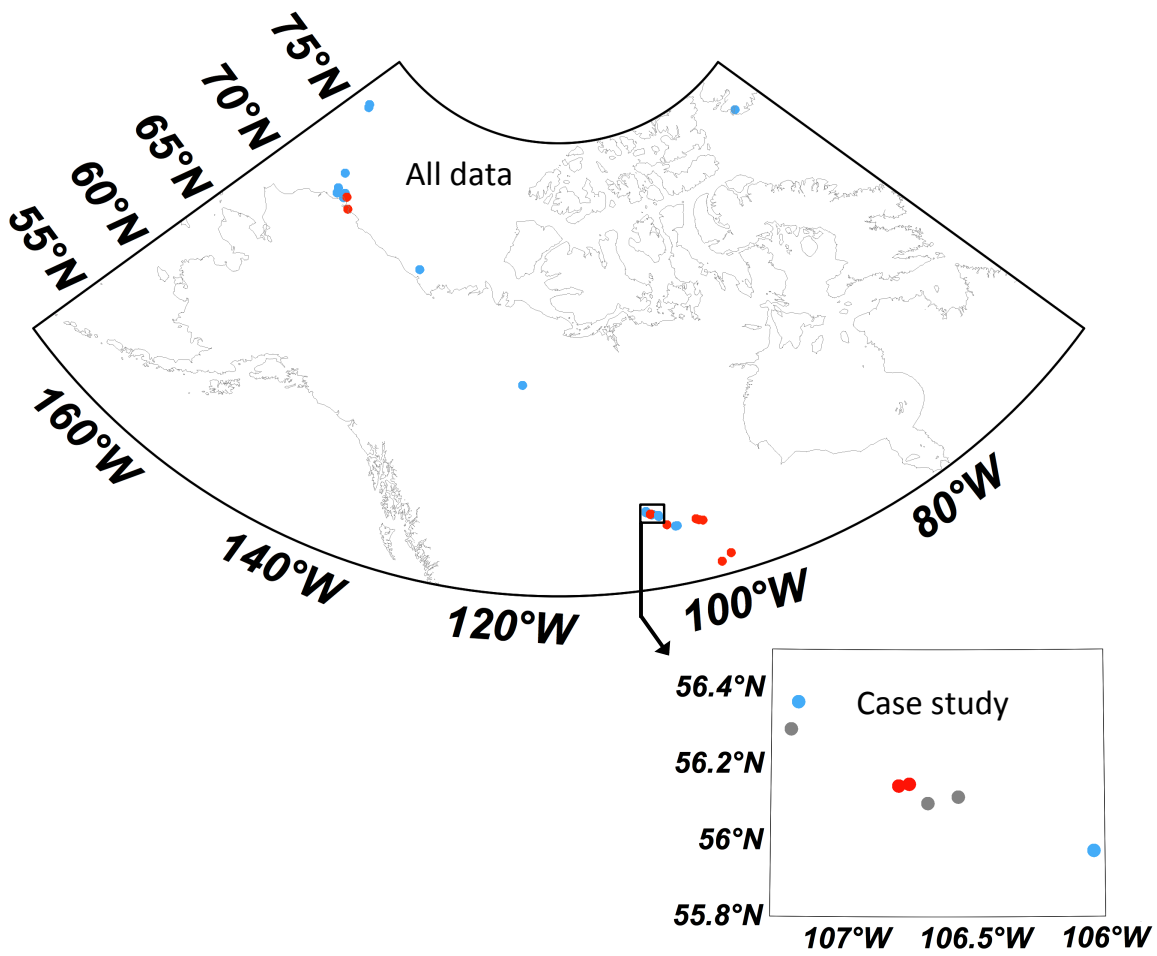
1
2
3
4
5
6
7
8
9

Figure 2. ISDAC 2008 aerosol and flight characteristics near and in selected clouds influenced by biomass burning from 19 April (left) and 20 April (right). Flight characteristics shown include: a) altitude, b) LWC (blue) and IWC (pink), c) aerosol concentration from the PCASP (black), SPLAT (red), and UHSAS (green) instruments, and d) bulk aerosol SPLAT chemical composition. Tan shading indicates SPLAT sampling through the in-cloud CVI inlet.



1
2

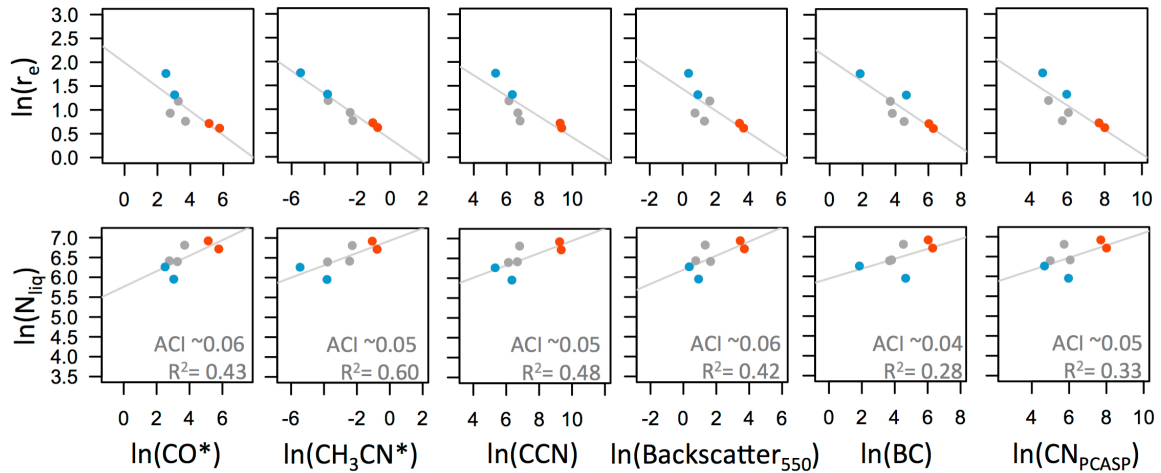
3 Figure 3. Carbon monoxide (ppbv) during the 1 July 2008 ARCTAS-B flight as a
4 function of a) the biomass burning tracer CH₃CN (ppbv) and b) the fossil fuel combustion
5 tracer CH₂Cl₂ (pptv).



1

2

3 Figure 4. Map of cloud sample locations from all campaigns. Red points indicate
 4 biomass burning samples, blue cases indicate background samples, and grey points
 5 indicate intermediate samples.

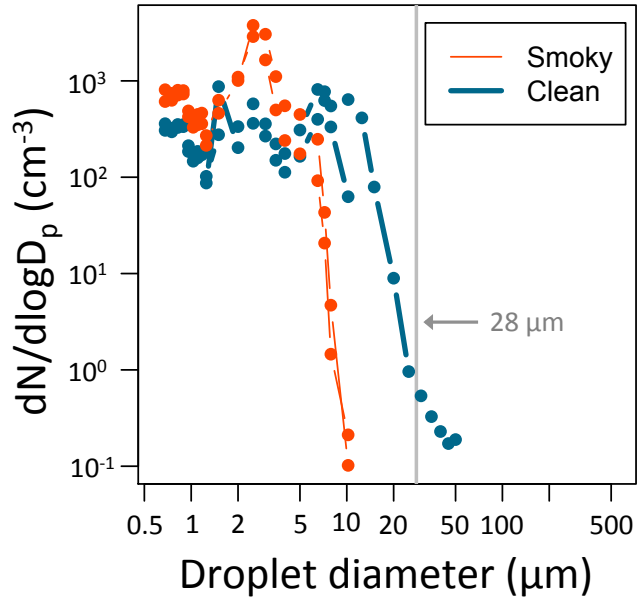


1

2

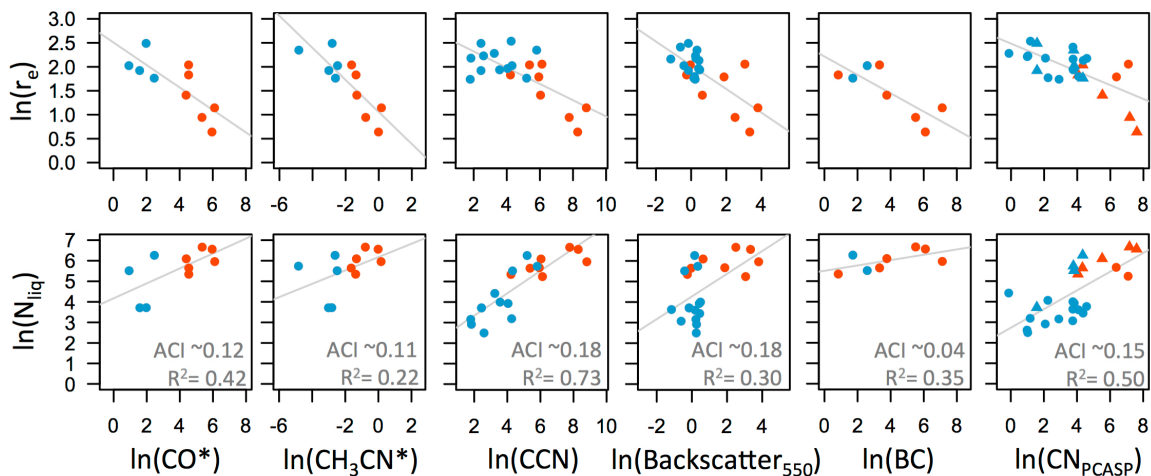
3 Figure 5. Based on seven samples from the ARCTAS-B 1 July 2008 case study, here we
 4 show the relationships between $\ln(r_e)$ (top row) and $\ln(N_{liq})$ (bottom row) and $\ln(BB_t)$
 5 derived from six indicators (where $BB_t = CO$ (ppbv) (* indicates background values of
 6 99.2 ppbv have been subtracted), CH_3CN (ppbv) (* indicates background values of 0.088
 7 ppbv have been subtracted), CCN (cm^{-3}), backscatter at 550 nm (Mm^{-1}), BC ($\mu g C m^{-3}$),
 8 and CN_{PCASP} equivalent values (cm^{-3}), as calculated from UHSAS and APS
 9 measurements. Biomass burning samples are noted in red, and background samples are
 10 noted in blue. To show variation between tracers, linear regressions and associated ACI
 11 estimates are shown in light gray (but note that final ACI values are not derived from
 12 individual regressions, but rather a combination of all six tracers).

13



1
2

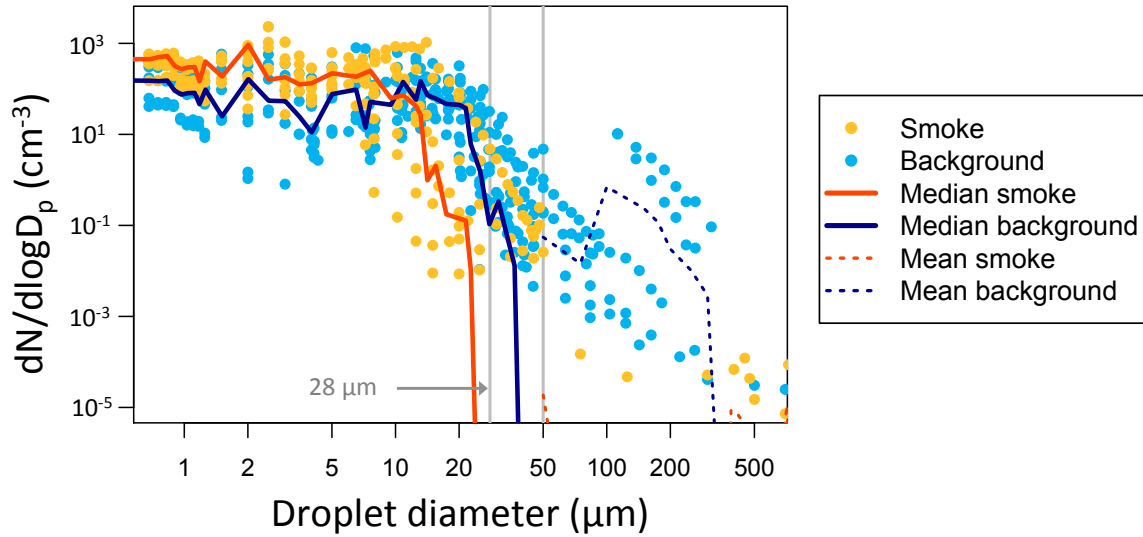
3 Figure 6. Mean cloud droplet size distributions (μm) for individual case study biomass
 4 burning clouds (thin orange lines) and clean background clouds (thick blue lines). The
 5 $28 \mu\text{m}$ line is marked in grey.



1
2

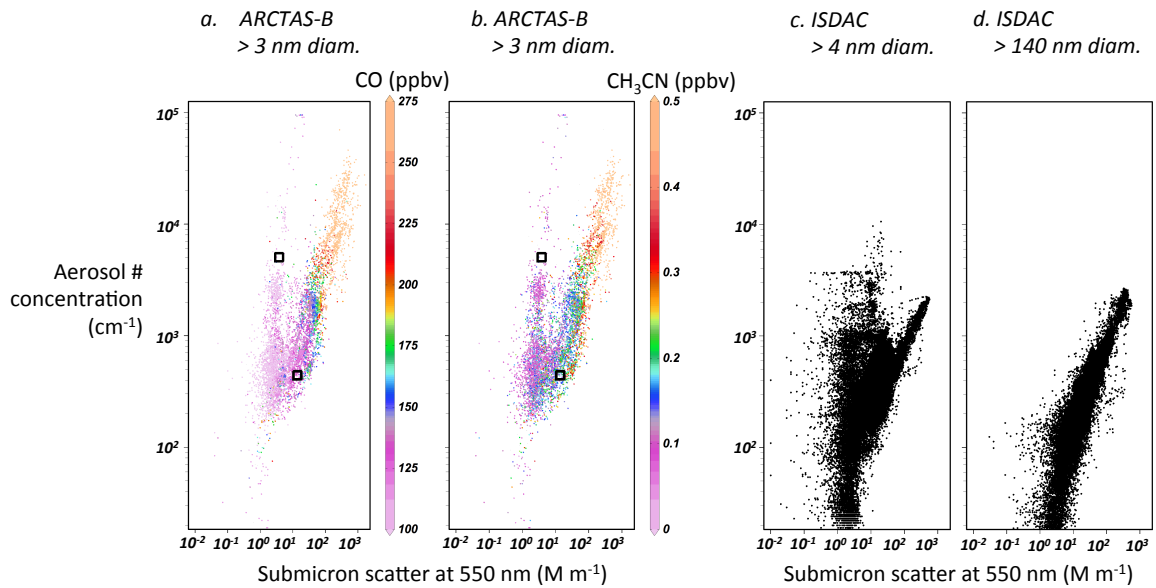
3 Figure 7. Same as in Fig. 5, but for data from the multi-campaign analysis. As in Figure
 4 5, CO* indicates that background values of 99.2 ppbv have been subtracted. For CH₃CN,
 5 the * indicates background values of 0.018 ppbv have been subtracted (due to low
 6 background CH₃CN levels in some of the samples).

7

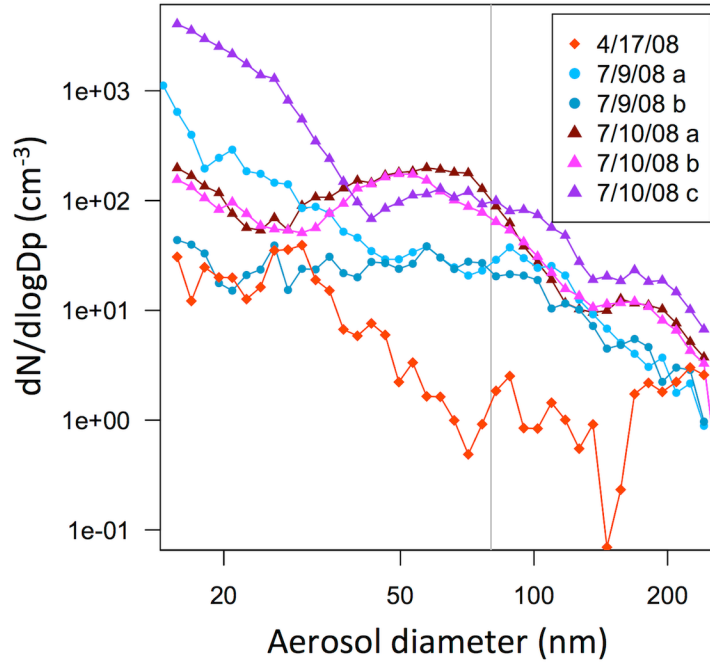


1
2

3 Figure 8. Mean cloud particle size distributions (μm) for all non-case study biomass
 4 burning clouds (yellow dots) and clean background clouds (light blue dots). The 28 and
 5 $50 \mu\text{m}$ lines are marked in grey. Thick red and darker blue lines indicate median values
 6 for binned size classes for smoky and clean clouds, respectively, including zero values
 7 not shown on the log-log plot. Due to the high number of zero values above $>50 \mu\text{m}$
 8 diameter, the mean values above this level are also shown (dashed lines) for comparison.



1
 2 Figure 9. Log relationships between ARCTAS-B and ISDAC aerosol number
 3 concentration and submicron scatter. In panels a and b, the combustion tracer CO, and
 4 the biomass burning tracer CH₃CN in out-of-cloud air masses are also shown. The black
 5 squares in panels a and b indicate where background aerosol concentrations of 5000 cm⁻³
 6 and dilute smoke concentrations of 450 cm⁻³ would be relative to other points.
 7 Measurements are from the following instruments: a and b) TSI 3025, c) TSI 3775, and
 8 d) PCASP. ARCTAS-B summertime samples were taken at altitudes < 5.2 km; ISDAC
 9 samples were taken at < 3.65 km due to TSI 3025 instrument limitations. All quality-
 10 flagged data were excluded, as well as suspicious ISDAC values within 17 km and < 1 km
 11 altitude of the Fairbanks, Alaska airport. Very small background aerosols appear to
 12 dominate the high aerosol number concentration/ low scatter particles seen in a-c, as
 13 shown by their disappearance when a diameter cutoff of 140 nm is used (d).



1
2

3 Figure A1. Mean out-of-cloud aerosol particle size distributions for several ARCTAS
 4 background aerosol events. Some days had multiple background aerosol events; these are
 5 distinguished by color and the letters a-c. The light grey line shows the 80 nm cutoff
 6 used here to distinguish Aitken mode particles from accumulation mode particles.